LABORATORY BLOCK EXPERIMENTS WITH SIX DIFFERENT COMBINATIONS OF STRESSES AND ROCK FABRICS

Organization:	University of Utah
Recipient Organization:	Lawrence Livermore National Laboratory
DUNS Number:	009095365
Recipient Address:	7000 East Ave. Livermore, CA 94550
Award Number:	2-2446
Project Title:	Closing the loop between in situ stress complexity and EGS fracture complexity
Project Period:	10/01/2021 – 06/30/2025
Principal Investigator(s):	Matteo Cusini (PI) cusini1@llnl.gov Andrew Bunger (Co-PI) bunger@pitt.edu
Report prepared by:	Yunxing Lu (PITT) Andrwe Bunger (PITT)
Report Submitted by:	Matteo Cusini
Date of Report Submission:	January 30, 2025
Related milestones:	MILESTONE 4.4.1

This work was performed under the auspices of the U.S. Department of Energy by Lawrence Livermore National Laboratory under Contract DE-AC52-07NA27344.

1. Introduction

This report documents the block hydraulic fracturing experiments that were conducted as part of task 4 of Utah FORGE project 2-2446. First, the report describes the experimental setup designed to replicate Utah FORGE conditions. Then, it details an innovative testing protocol, including the examination of post-peak pressure records and the improved wellbore temperature measurement setup. Following this, a concise, enumerated summary of key findings is provided for each sample under various testing conditions, highlighting the main results obtained so far.

2. Methodologies

2.1 The Experimental Matrix with 6 Different Combinations and Their Notations

Building on the success of performance period 1, we designed and conducted 17 experimental tests on 6-inch cubic granite samples relevant to the Utah FORGE site conditions by the end of the performance period 2. These tests can be categorized into 6 classes based on different well directions, in-situ stress regimes and ratios, and thermal stress conditions:

a) Vertical well-Room temperature sample-No-Thermal Stress (VR-NTS)

b) Vertical well-High temperature sample-No-Thermal Stress (VH-NTS)

c) Vertical well-High temperature sample-Induced Thermal Stress (VH-ITS)

d) Inclined well-High temperature sample-Induced Thermal Stress (IH-ITS)

e) Horizonal well-High temperature sample-Induced Thermal Stress (HH-ITS)

f) Horizonal well-Room temperature sample-No-Thermal Stress (HR-NTS)

For the notation above, the vertical well indicates that the well direction is aligned with the vertical stress, whereas the horizontal well indicates that the well direction is parallel with the horizontal minimum stress. The high-temperature sample means the granite sample is heated to 190-200 °C when the test starts. Room temperature sample means the hydraulic fracturing test is performed on the room temperature granites, and for these room temperature cases, there is no thermal stress induced since the thermal stress is induced by circulating room temperature water through the hot sample to create the thermal gradient. Each test has been enabled the extended analysis of post-peak pressure behaviors, which assists in post-test pressure analyses such as the G-function, step rate, and rapid reopening tests. These additional measurements are designed to improve the identification of key components constituting the in-situ stresses. Ultimately, these enhancements should lead to more accurate estimates of in-situ stresses.

2.2 True Triaxial High-Temperature (Up to 200°C) Hydraulic Fracturing Block Test Setup Relevant to Utah FORGE Conditions and Its Testing Protocols

The experimental setup involves testing 6-inch cubic granite blocks under two scenarios—room temperature and 200 degrees Celsius—using a hydraulic piston-actuated loading cell under true triaxial loading conditions with various combinations of in-situ stress. The St. Cloud Gray granodiorite is used here as the FORGE-analogue granite for laboratory testing purposes. This selection is primarily founded on acoustic anisotropy properties, assessed and calculated using the acoustic transmission system. This system can measure both S and P waves as they traverse the test sample. The velocity of these waves can serve as an indicator of the granite's anisotropy. To promote an even distribution of stress on the testing sample, aluminum loading plates with a minimum thickness of 3 inches are inserted between each side of the sample and the tilt saddle on the actuator. To further mitigate friction and prevent shear boundary conditions, Teflon sheets are placed between each face of the sample and the aluminum loading plate. For the second testing case, where the host block is heated to 200 degrees Celsius, thermal stress can be induced within the sample near the borehole by circulating room-temperature water through the borehole. As shown in Figure 1, this process results in a temperature drop of up to 140-150 degrees Celsius at the borehole wall when the circulation starts. The circulation time lasts around 15 minutes. During this time, a total of 2-4 liters of water is circulated through the borehole, and the borehole temperature continues to decrease, albeit at a slower rate, by approximately another 10 to 20°C. When the circulation is stopped, it waits for a period of time for the borehole temperature to recover to a relatively stable value. Then, the system's outlet is closed to initiate the hydraulic fracturing process. In the scenario without thermal stress, the hydraulic fracturing starts immediately after bleeding the air out of the system.

During the hydraulic fracturing phase, the fluid is injected into the wellbore at a constant flow rate of 3 ml/min until the breakdown pressure is reached. After that, the injection is stopped and the wellbore pressure is monitored to observe post-peak pressure decline behaviors, which are referred to as the shut-in phase. The shut-in phase commences when the borehole pressure stabilizes at a constant value. After the shut-in phase, a reopening test is performed by injecting the same fluid at the same flow rate into the borehole to observe pressure responses. Similarly, when the pressure reaches the peak in the reopening test, another shut-in phase is implemented. The procedure then moves to the step-rate pressure test, during which the borehole pressure increases in increments of 0.68 MPa (100 psi). Each subsequent step commences only after the current pressure level has stabilized at a constant flow rate. At each stage, the pressure level and corresponding flow rate are recorded and plotted for future analysis. Following the step-rate phase, another shut-in period occurs, after which the wellbore pressure decreases to ambient levels. With these steps completed, the entire test procedure is considered finished. These three phases constitute the whole process of the post-peak wellbore pressure analysis, as shown in Figure 1, and have provided the opportunity to infer the reopening pressure and minimum horizontal stress at different angles.

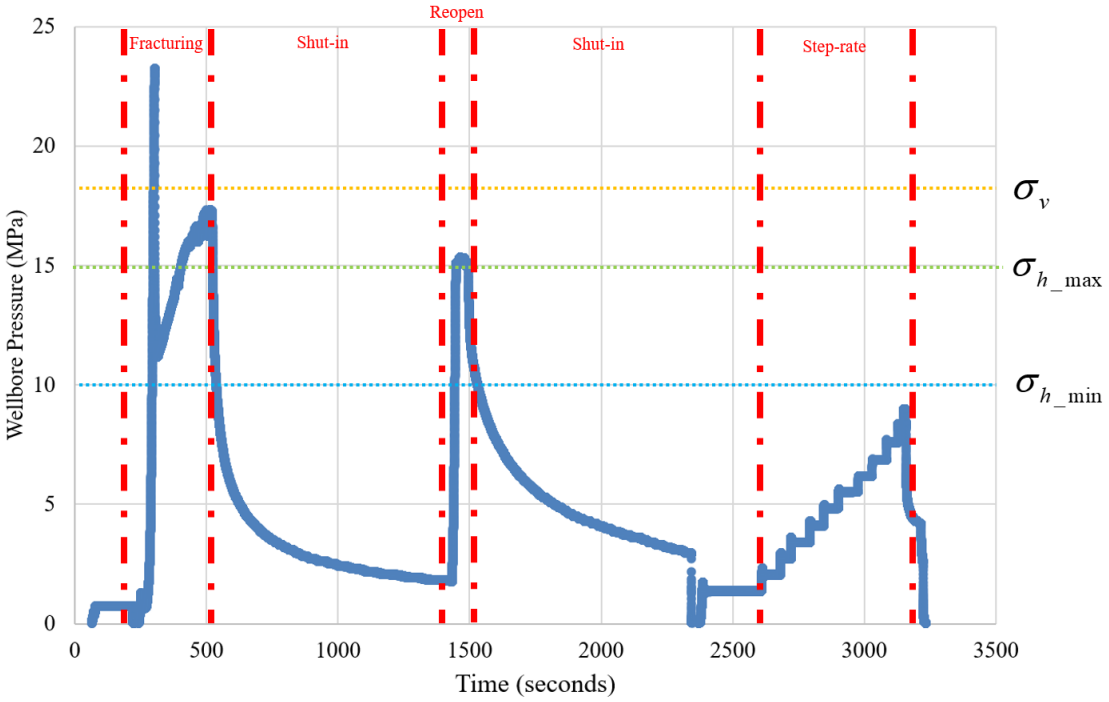

Figure 1. An example of full wellbore pressure record to show the lifecycle from fracturing to step rate testing.

2.3 Improved Temperature Measurements Device

In performance period 1, the borehole wall temperature was roughly estimated based on continuous assumptions about the temperature relationship between the borehole wall and the circulating fluid, relying primarily on the outlet fluid temperature for estimations. In performance period 2, as shown in Figure 2, improved and more precise temperature measurements were achieved by isolating the thermocouple tips from the circulating fluids, effectively reducing potential noise in the temperature data caused by environmental factors. Using a newly designed set of injection tools, repeated circulation tests were conducted to measure changes in borehole wall temperature during this period.

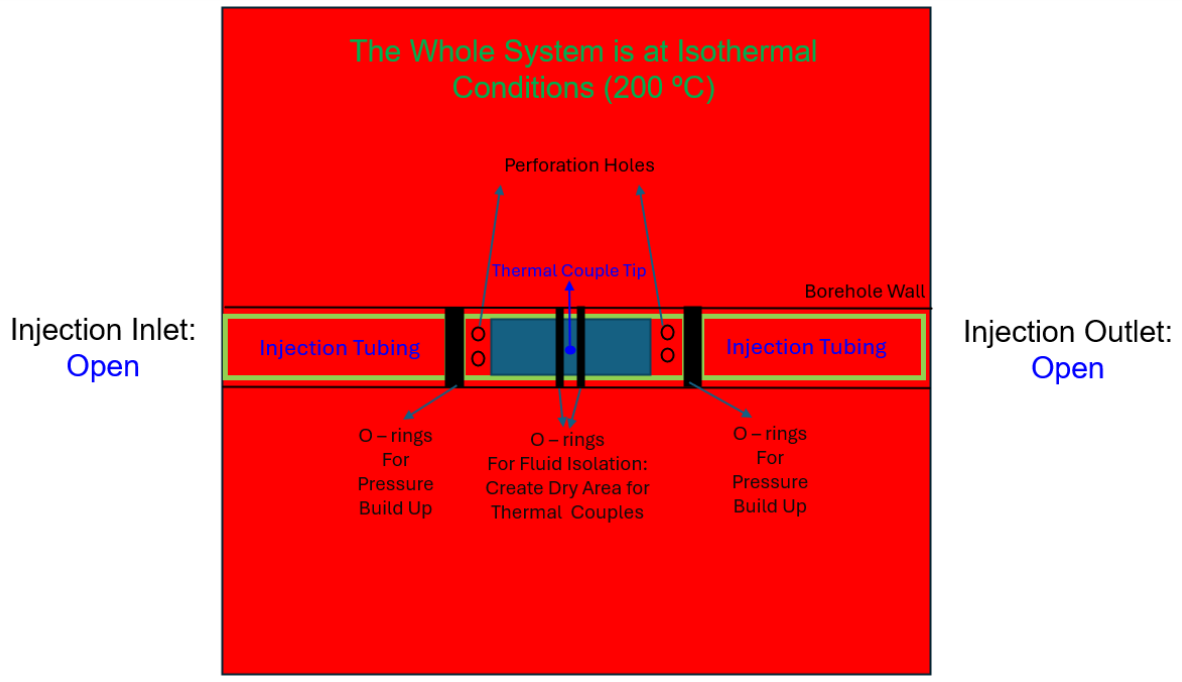

Figure 2. Illustration of the enhanced wellbore temperature measurement setup

3. Results

For all vertical well cases, the detailed experimental data has been reported in previous milestone reports, Milestones 4.1.1 and 4.2.1. Therefore, only the horizontal well dataset is presented in this milestone report.

3.1 HH-ITS-1

The HH-ITS-1 is performing hydraulic fracturing at an elevated temperature (around 200 degrees Celsius) with induced thermal stress and in-situ stress (vertical stress = 17.5 MPa, maximum horizontal stress = 15 MPa, minimum horizontal stress = 10 MPa). Figure 4(a) shows the full pressure record during the four phases of stimulation: hydraulic fracturing, shut-in, reopening, and step rate. The breakdown pressure in this case is 23.1 MPa. Using the fracture compliance method, the G-function plot (Figure 4b) from the first shut-in period indicates that the closure pressure is around 15 MPa from compliance method and 14 MPa from tangent method, whereas the closure pressures picked up from rapid reopening test (Figure 4c) and step rate test (Figure 4d) are around 18.5 MPa and 15.5 MPa, respectively. Fracture patterns on the surface of the 6-inch cube from the HH-ITS-1 testing case are observed as mixed type, as it has both longitudinal and transverse fractures, as shown in Figure 5. However, the fracture observations on the 2-inch post-test over-core show that it appears the fracture initially starts longitudinally from

the center of the core, as shown in Figure 6. As it propagates toward the end of the core, it deviates into the transverse direction.

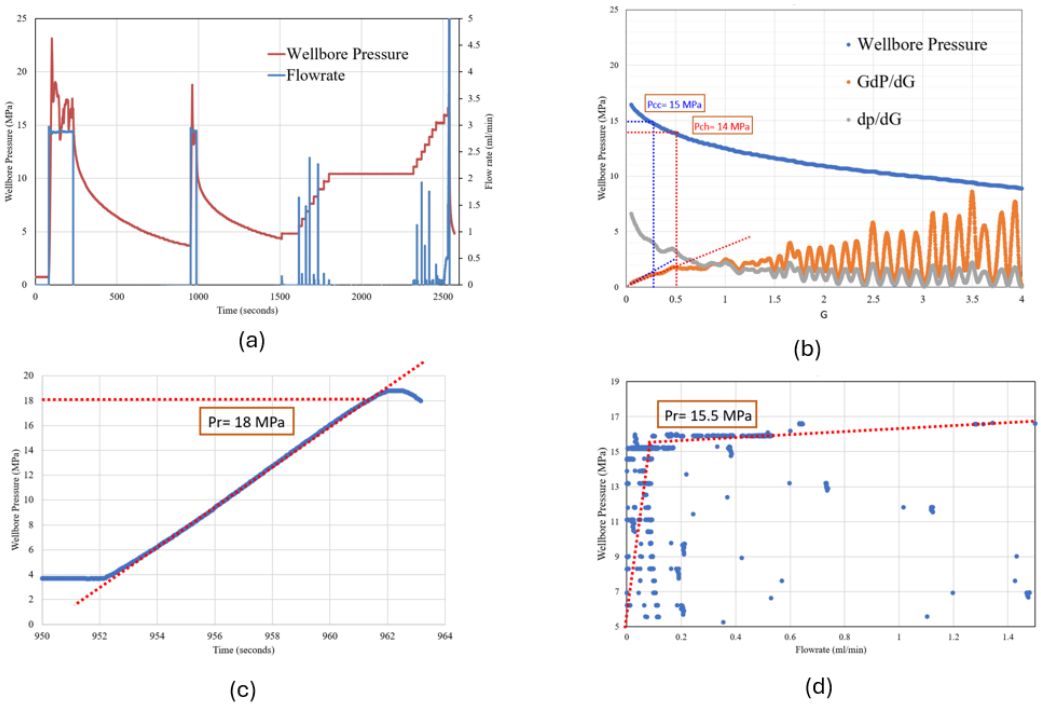

Figure 4. HH-ITS-1: (a) Full wellbore pressure record (primary y axis is the wellbore pressure and secondary y axis is flow rate); (b) G-function plot (Pcc from compliance method and Pch from tangent method); (c) Step rate plot; (d) Reopening test pressure record.

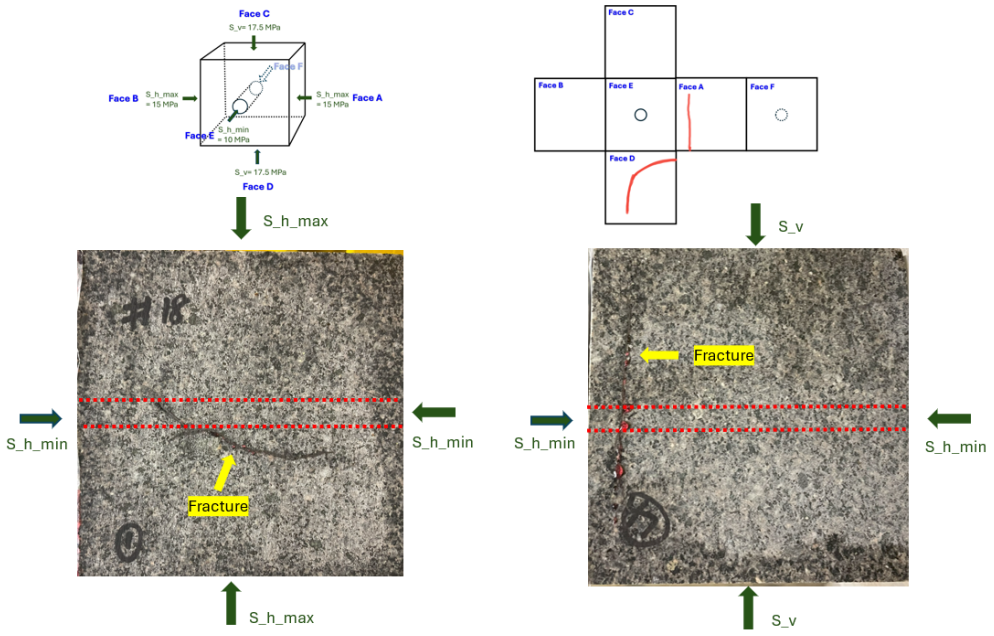

Figure 5. Observations of fracture patterns on the surface of the 6-inch cube from the HH-ITS-1 testing case.

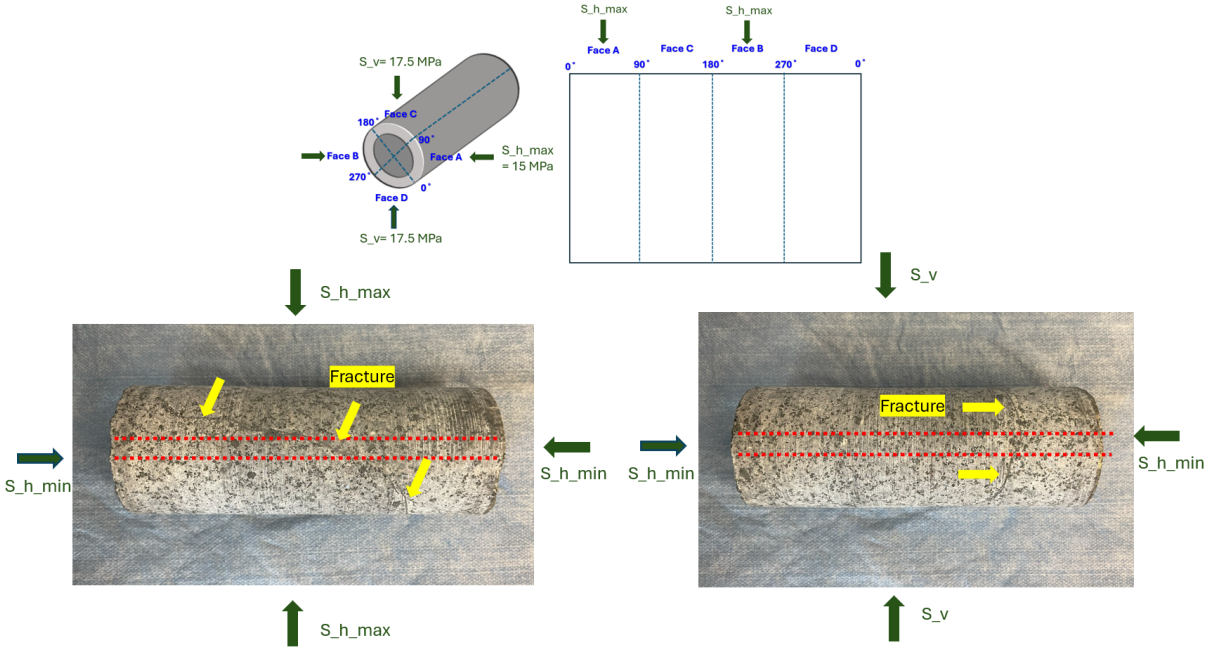

Figure 6. Observations of fracture patterns on the surface of the 2-inch core from the HH-ITS-1 testing case.

3.2 HH-ITS-2

Unlike the previous case, HH-ITS-1, HH-ITS-2 is performing hydraulic fracturing at an elevated temperature (around 200 degrees Celsius) with induced thermal stress but with a smaller level of minimum horizontal stress, which is 3 MPa, while the vertical stress and maximum horizontal stress remain the same at 17.5 MPa and 15 MPa, respectively. Figure 7(a) shows the full pressure record during the four phases of stimulation: hydraulic fracturing, shut-in, reopening, and step rate. The breakdown pressure in this case is 21.4 MPa. Using the fracture compliance method, the G-function plot (Figure 7b) from the first shut-in period indicates that the closure pressure is around 7.5 MPa. By using the tangent method, the closure pressure is estimated around 5.5 MPa. The reopening pressure picked up from rapid reopening tests (Figure 7c) and step rate test (Figure 7d) are both around 10 MPa. Fracture patterns observed on both the surface of the 6-inch cube and the 2-inch core are found to be transverse patterns, as shown in Figures 8 and 9.

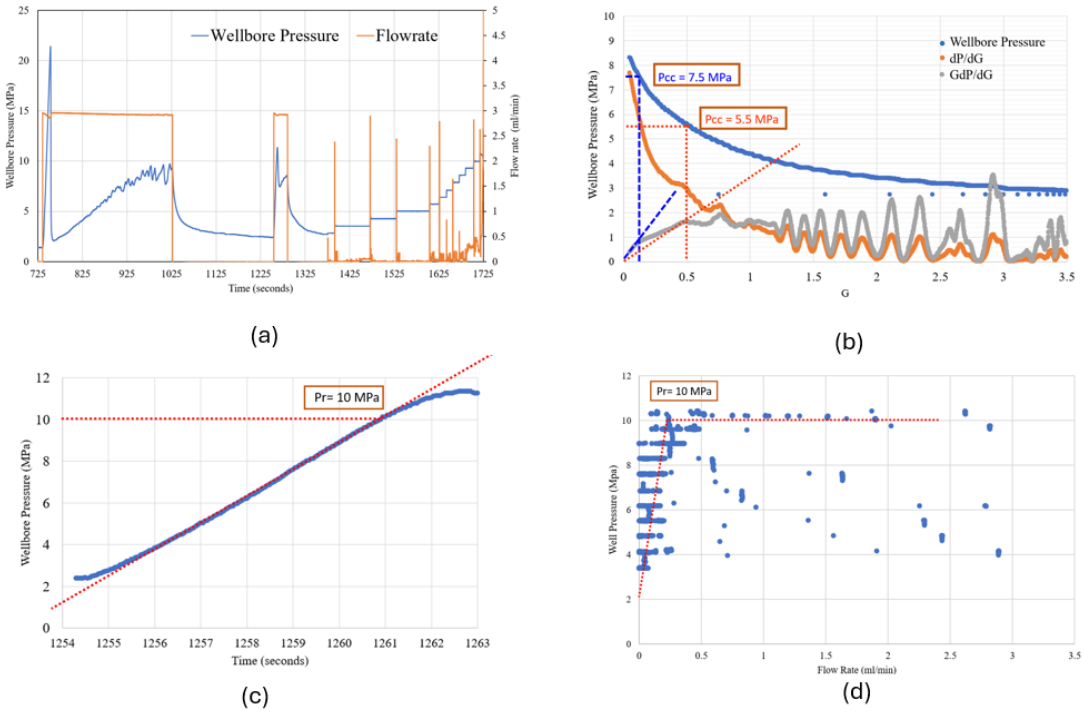

Figure 7. HH-ITS-2: (a) Full wellbore pressure record (primary y axis is the wellbore pressure and secondary y axis is flow rate); (b) G-function plot Pcc from compliance method and Pch from tangent method; (c) Step rate plot; (d) Reopening test pressure record.

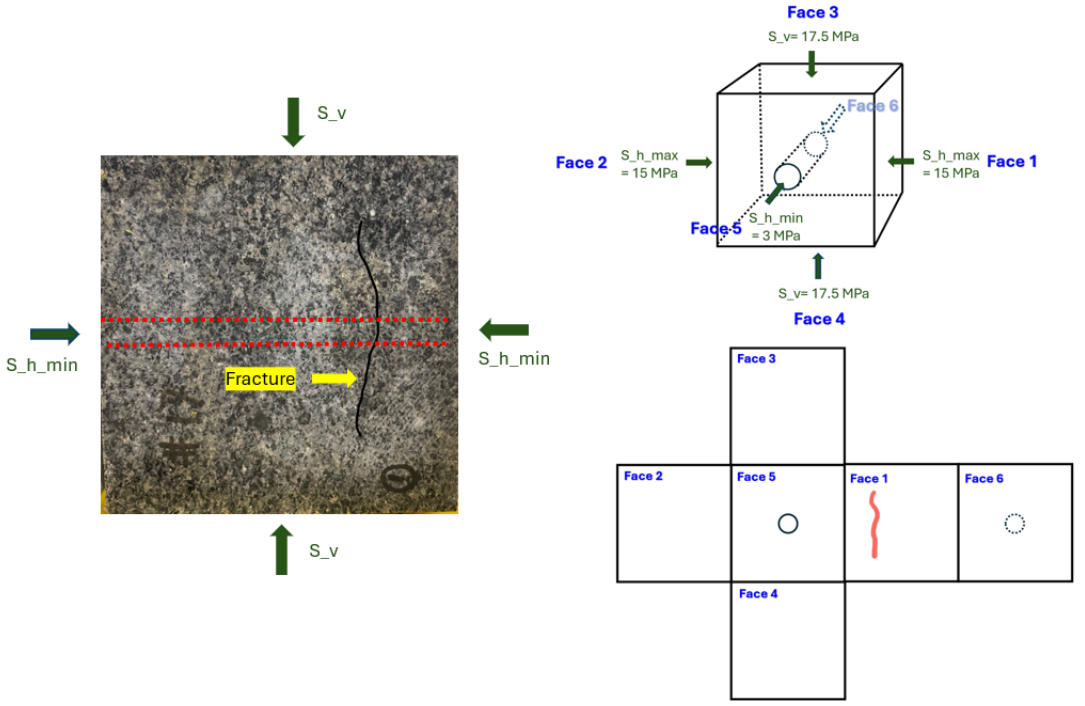

Figure 8. Observations of fracture patterns on the surface of the 6-inch cube from the HH-ITS-2 testing case.

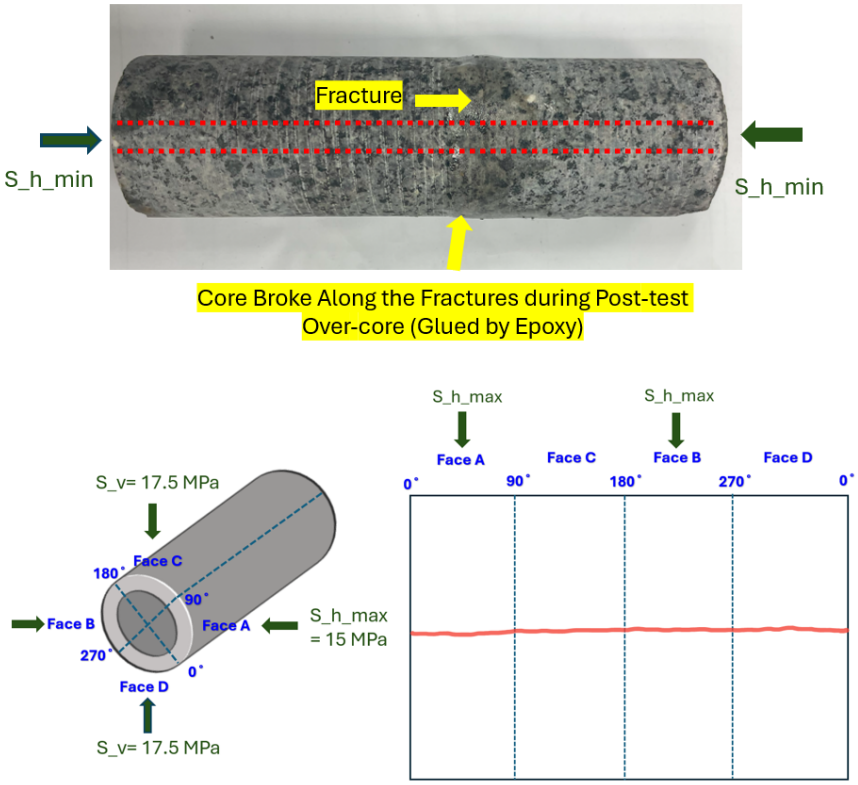

Figure 9. Observations of fracture patterns on the surface of the 2-inch core from the HH-ITS-2 testing case.

3.3 HH-ITS-3

The HH-ITS-3 is directly repeated test of the HH-ITS-2 under the same condition. Figure 10(a) shows the full pressure record during the four phases of stimulation: hydraulic fracturing, shut-in, reopening, and step rate. The breakdown pressure in this case is 11 MPa. Using the fracture compliance method, the G-function plot (Figure 10b) from the first shut-in period indicates that the closure pressure is around 6 MPa. By using the tangent method, the closure pressure is estimated around 4 MPa. The reopening pressures picked up from the rapid reopening test (Figure 10c) and step rate test (Figure 10d) are both around 5 MPa. Fracture patterns observed on both the surface of the 6-inch cube and the 2-inch core are found to be mixed patterns, as shown in Figures 11 and 12.

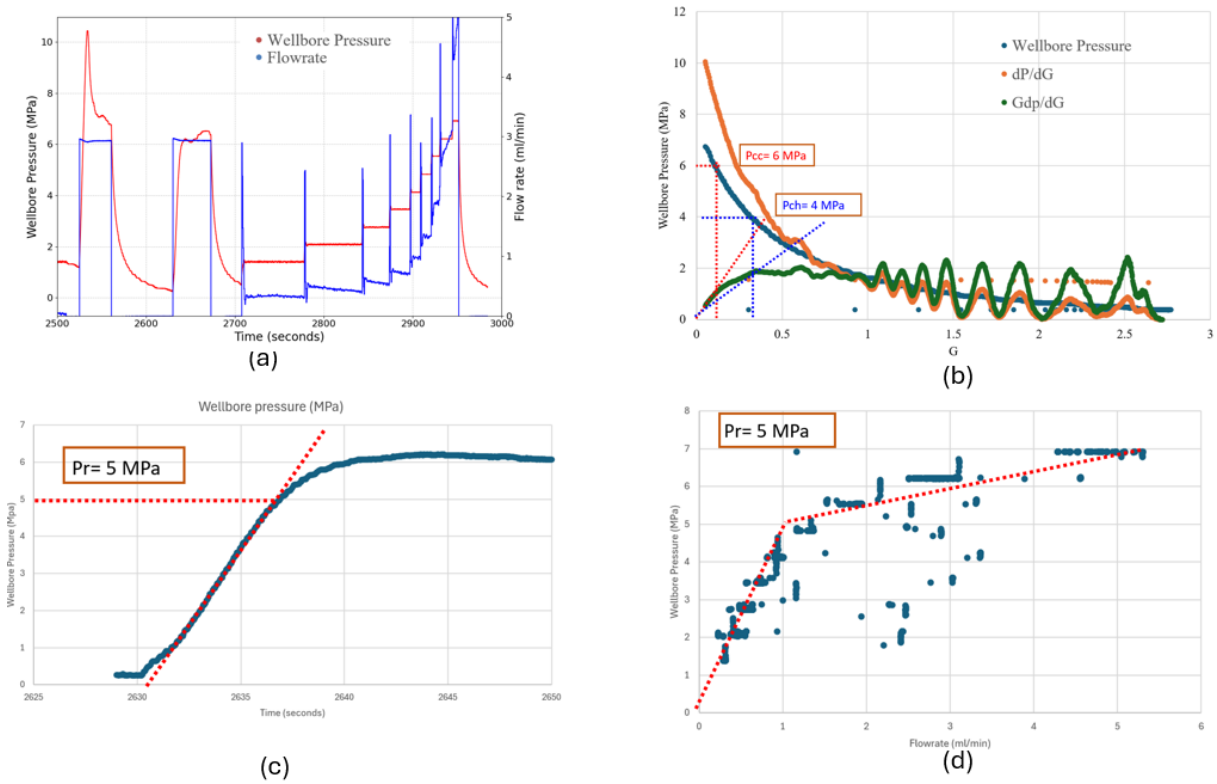

Figure 10. HH-ITS-3: (a) Full wellbore pressure record (primary y axis is the wellbore pressure and secondary y axis is flow rate); (b) G-function plot (Pcc from compliance method and Pch from tangent method); (c) Step rate plot; (d) Reopening test pressure record.

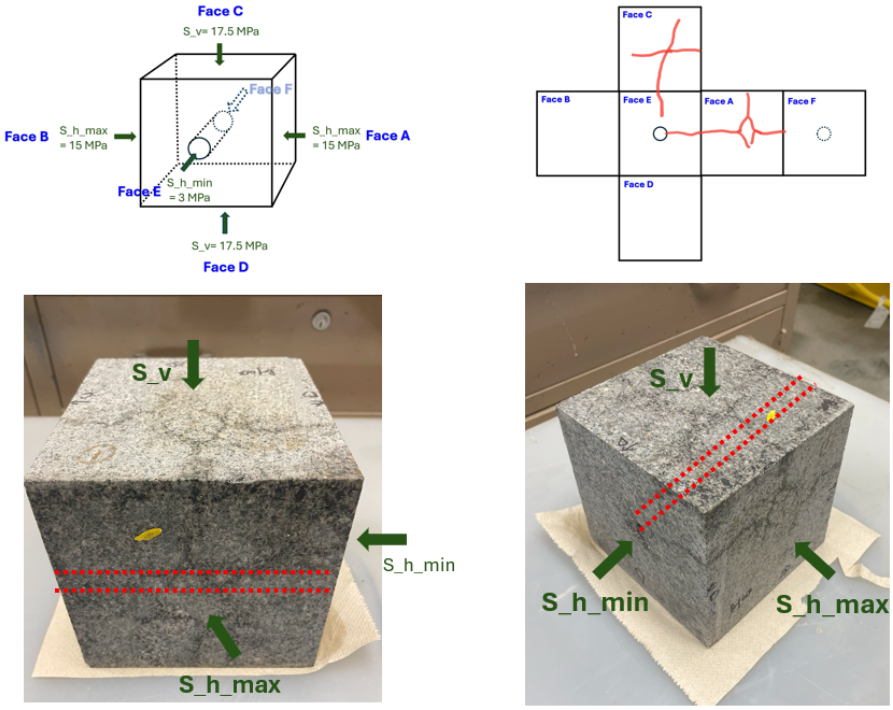

Figure 11. Observations of fracture patterns on the surface of the 6-inch cube from the HH-ITS-3 testing case.

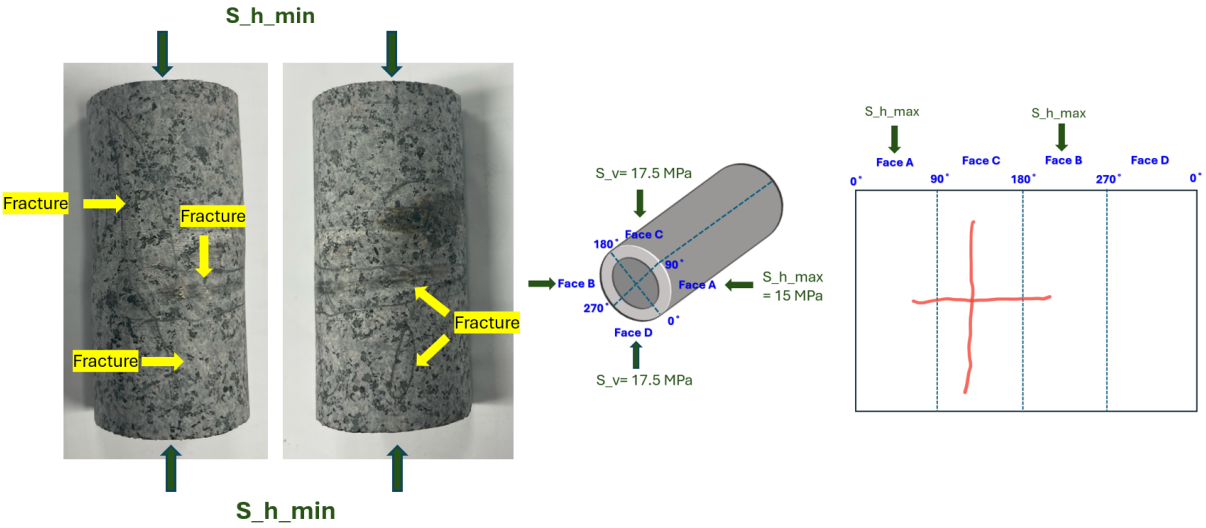

Figure 12. Observations of fracture patterns on the surface of the 2-inch core from the HH-ITS-3 testing case.

3.4 HH-ITS-4

For HH-ITS-4, this experiment is performing hydraulic fracturing at an elevated temperature (around 200 degrees Celsius) with induced thermal stress but with a medium level of minimum horizontal stress (7 MPa) compared with the previous testing case, while the vertical stress and maximum horizontal stress remain the same at 17.5 MPa and 15 MPa, respectively. Figure 11(a) shows the full pressure record during the four phases of stimulation: hydraulic fracturing, shut-in, reopening, and step rate. The breakdown pressure in this case is 15 MPa. Using the fracture compliance method, the G-function plot (Figure 13b) from the first shut-in period indicates that the closure pressure is around 10 MPa. By using the tangent method, the closure pressure is estimated around 7 MPa. The reopening pressure picked up from the rapid reopening test (Figure 11c) and step rate test (Figure 11d) are both around 9 MPa. Fracture patterns observed on both the surface of the 6-inch cube and the 2-inch core are found to be transverse patterns, as shown in Figures 12 and 13.

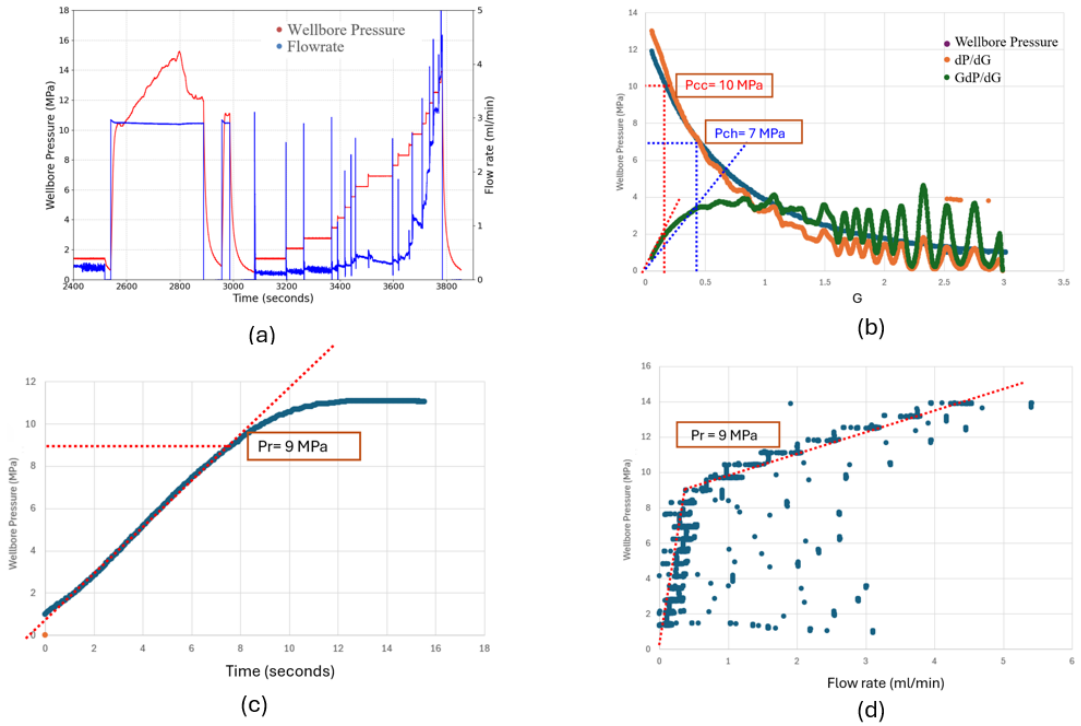

Figure 11. HH-ITS-4: (a) Full wellbore pressure record (primary y axis is the wellbore pressure and secondary y axis is flow rate); (b) G-function plot (Pcc from compliance method and Pch from tangent method); (c) Step rate plot; (d) Reopening test pressure record

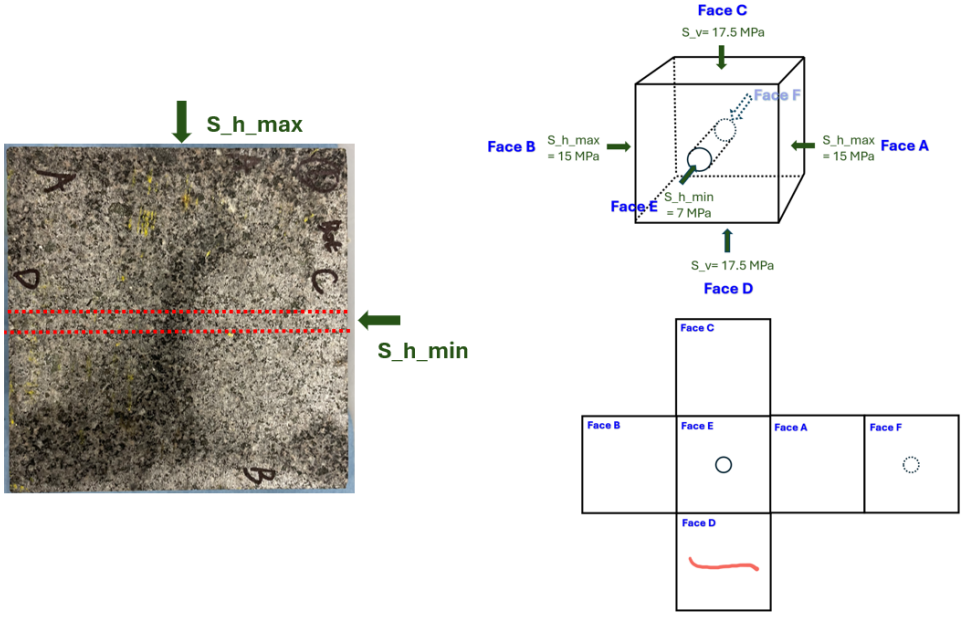

Figure 12. Observations of fracture patterns on the surface of the 6-inch cube from the HH-ITS-4 testing case.

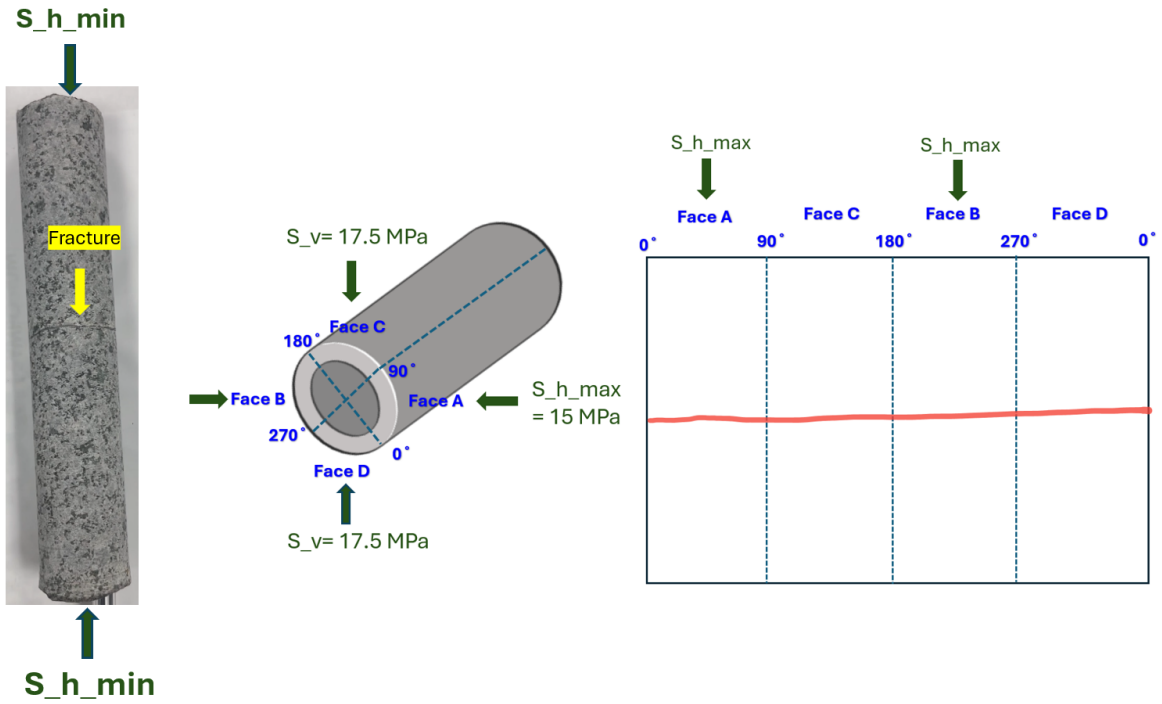

Figure 13. Observations of fracture patterns on the surface of the 2-inch core from the HH-ITS-4 testing case.

3.5 HR-NTS-1

For HR-NTS-1, this experiment involves performing hydraulic fracturing at room temperature without inducing any thermal stress. The in-situ stresses are maintained at a vertical stress of 17.5 MPa, a maximum horizontal stress of 15 MPa, and a minimum horizontal stress of 3 MPa. Figure 14(a) shows the full pressure record during the four phases of stimulation: hydraulic fracturing, shut-in, reopening, and step rate. The breakdown pressure in this case is 37.5 MPa. Using the fracture compliance method, the G-function plot (Figure 14b) from the first shut-in period indicates that the closure pressure is around 11 MPa. By using the tangent method, the closure pressure is estimated around 6.5 MPa. The reopening pressures obtained from the rapid reopening test (Figure 14c) and step rate (Figure 14d) are both around 11-12 MPa. Fracture patterns observed on the surface of the 6-inch cube are inclined, while those on the surface of the 2-inch core are of the bi-wing longitudinal type as shown in both Figure 15 and 16.

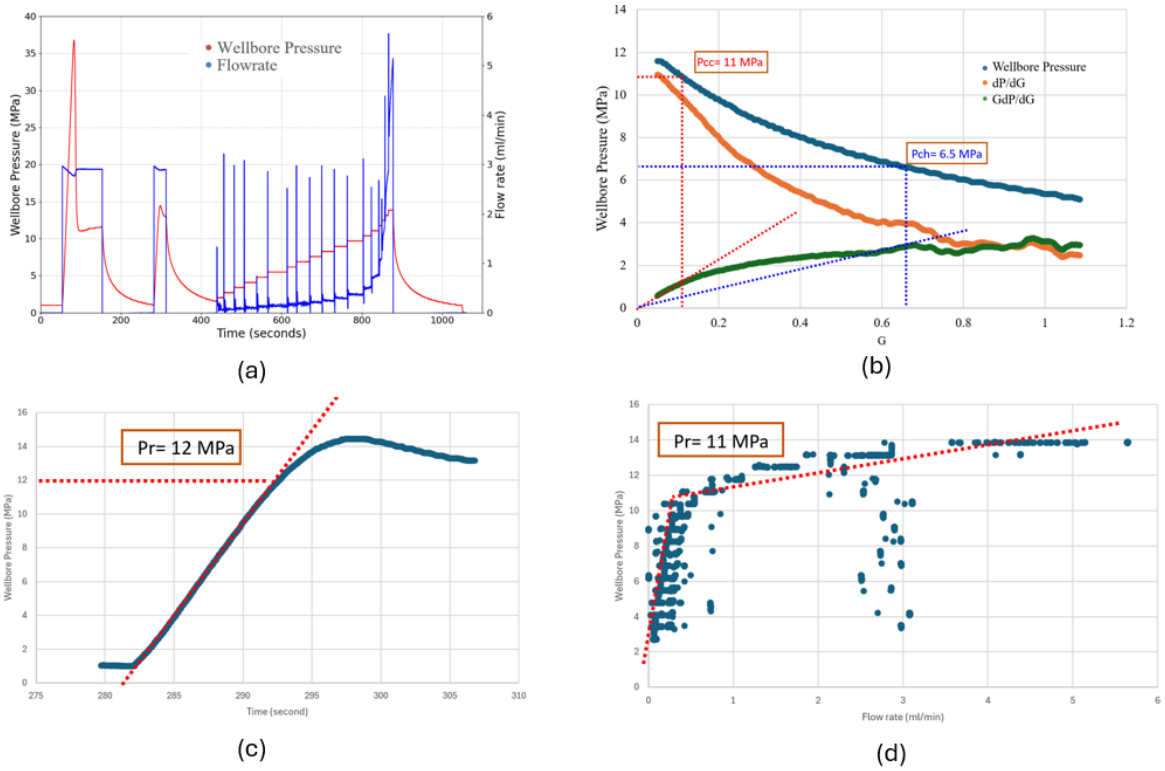

Figure 14. HR-NTS-1: (a) Full wellbore pressure record (primary y axis is the wellbore pressure and secondary y axis is flow rate); (b) G-function plot (Pcc from compliance method and Pch from tangent method); (c) Step rate plot; (d) Reopening test pressure record

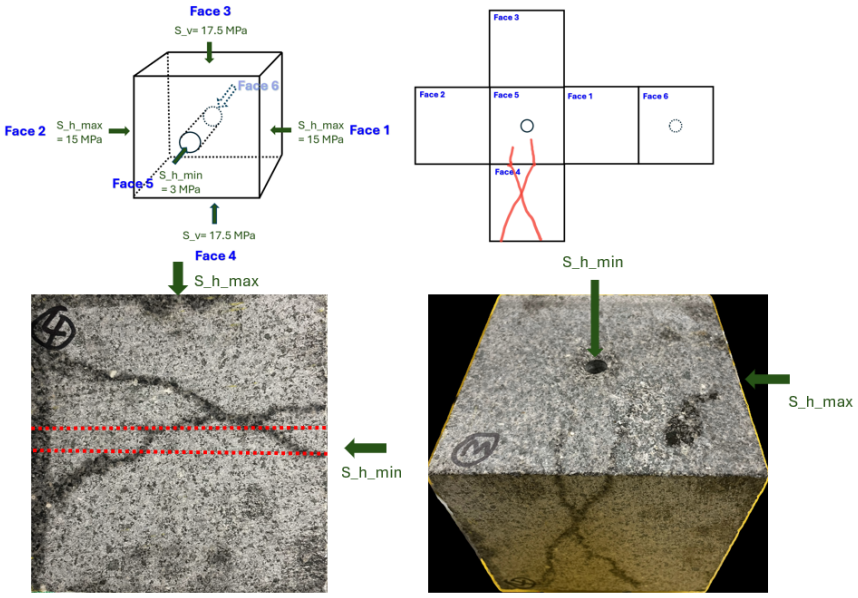

Figure 15. Observations of fracture patterns on the surface of the 6-inch cube from the HR-NTS-1 testing case.

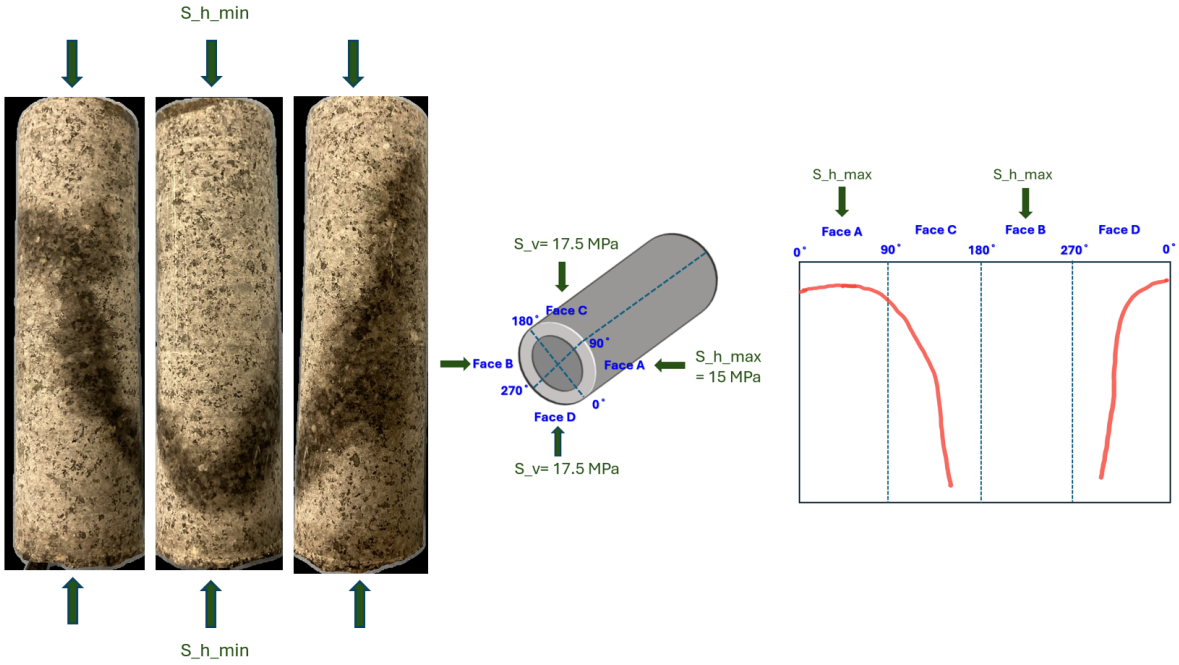

Figure 16. Observations of fracture patterns on the surface of the 2-inch core from the HR-NTS-1 testing case.

3.6 HR-NTS-2

The experiment HR-NTS-2 is a direct repeat of HR-NTS-1 with exactly the same conditions. Figure 17(a) shows the full pressure record during the four phases of stimulation: hydraulic fracturing, shut-in, reopening, and step rate. The breakdown pressure in this case is 42.5 MPa. Using the fracture compliance method, the G-function plot (Figure 17b) from the first shut-in period indicates that the closure pressure is around 11 MPa and by using the tangent method the fracture closure pressure is estimated as 7.8 MPa. The reopening pressures obtained from the rapid reopening test (Figure 17c) and step rate test (Figure 17d) are approximately 14MPa and 13 MPa, respectively. Fracture patterns observed on the surface of the 6-inch cube show a 45-degree inclination, while the fracture pattern observed on the 2-inch core is longitudinal as shown in Figure 18 and 19.

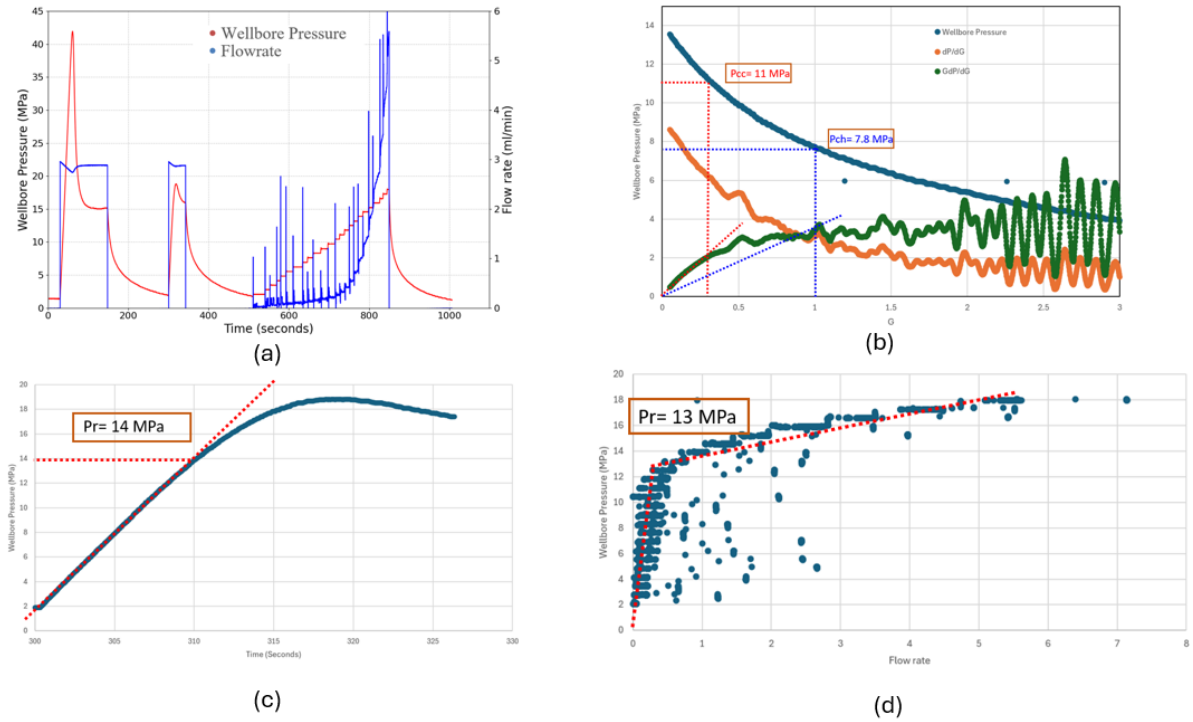

Figure 17. HR-NTS-2: (a) Full wellbore pressure record (primary y axis is the wellbore pressure and secondary y axis is flow rate); (b) G-function plot (Pcc from compliance method and Pch from tangent method); (c) Step rate plot; (d) Reopening test pressure record

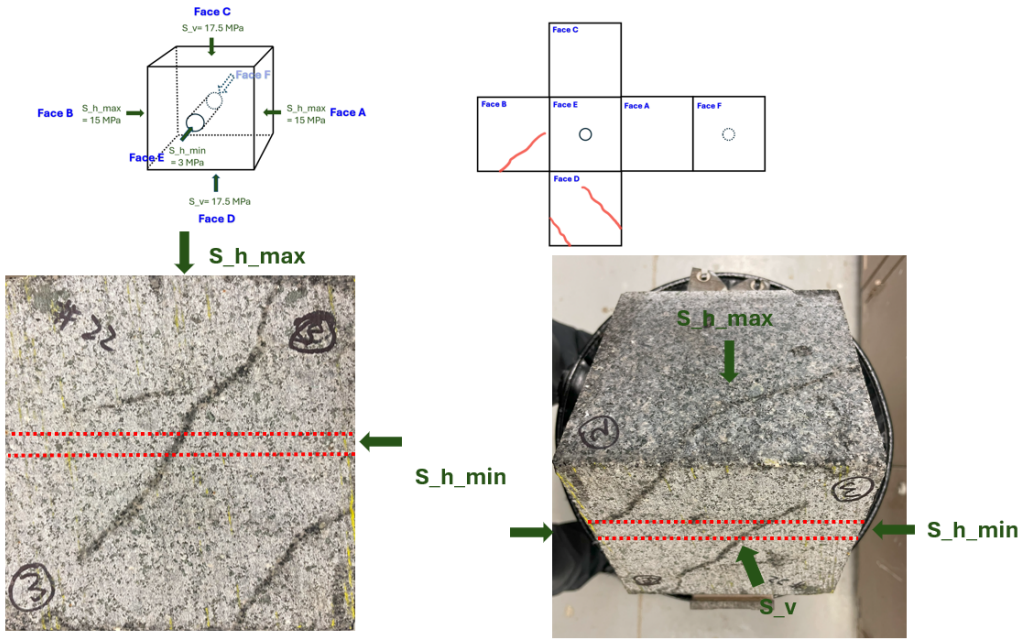

Figure 18. Observations of fracture patterns on the surface of the 6-inch cube from the HR-NTS-2 testing case.

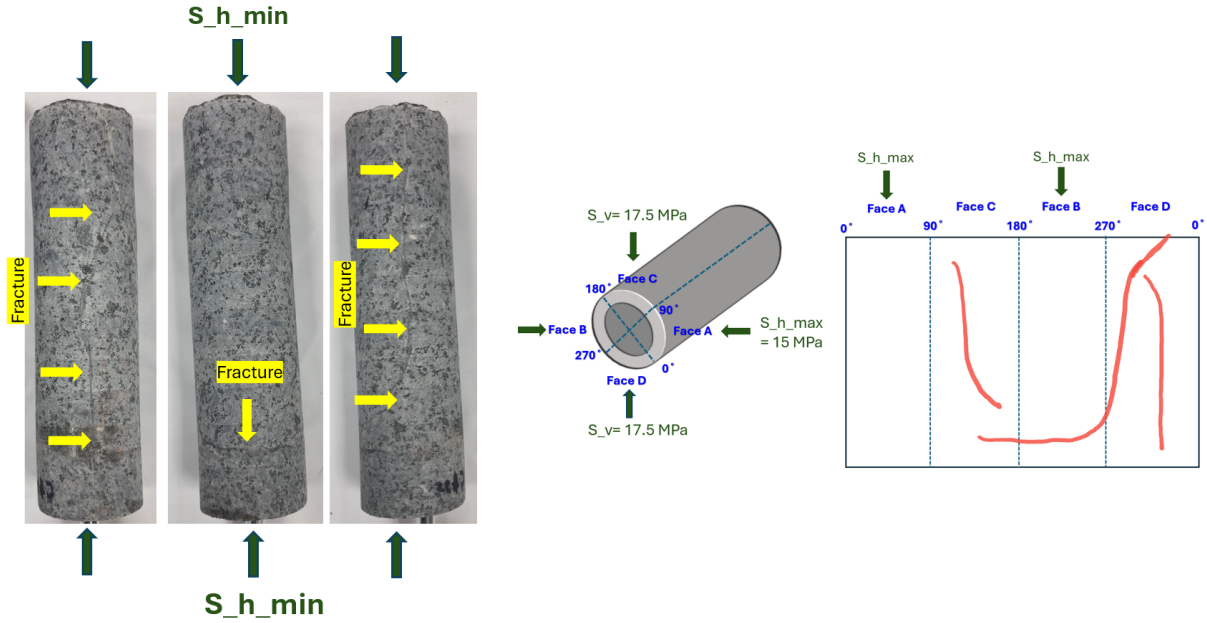

Figure 19. Observations of fracture patterns on the surface of the 2-inch core from the HR-NTS-2 testing case.

3.7 HR-NTS-3

Unlike the previous case, HR-NTS-3 is performed with a different level of minimum horizontal stress, which is 7 MPa, while the vertical stress and maximum horizontal stress remain the same at 17.5 MPa and 15 MPa, respectively and the experiment is performed at room temperature and without inducing any thermals stress. Figure 20 (a) shows the full pressure record during the four phases of stimulation: hydraulic fracturing, shut-in, reopening, and step rate. The breakdown pressure in this case is 20.4 MPa. Using the fracture compliance method, the G-function plot (Figure 20b) from the first shut-in period indicates that the closure pressure is around 7.5 MPa. By using the tangent method, the fracture closure pressure is estimated as 4.8 MPa. The reopening pressure picked up from the rapid reopening test (Figure 20c) and step rate test (Figure 20d) are both around 7 MPa. Fracture patterns observed on the surface of the 6-inch cube show a mixed type, while the fracture pattern observed on the 2-inch core is longitudinal as shown in Figure 21 and 22.

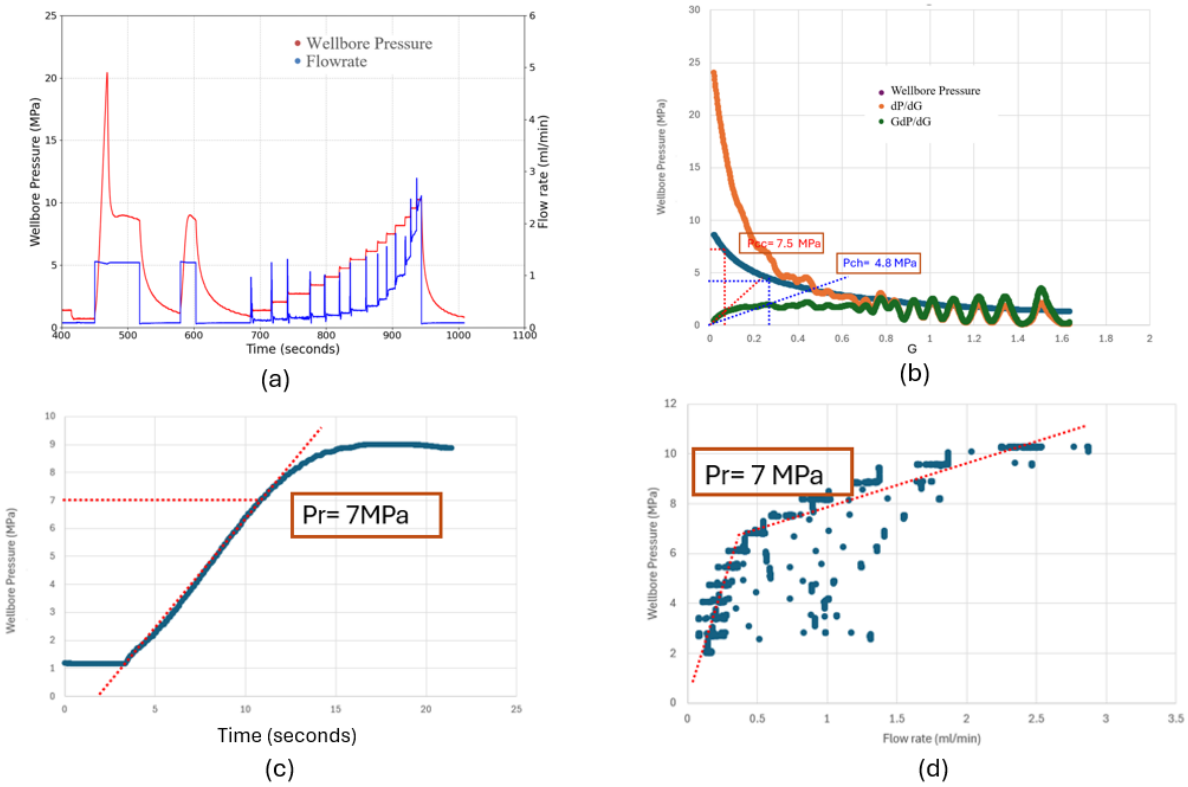

Figure 20. HR-NTS-3: (a) Full wellbore pressure record (primary y axis is the wellbore pressure and secondary y axis is flow rate); (b) G-function plot (Pcc from compliance method and Pch from tangent method); (c) Step rate plot; (d) Reopening test pressure record

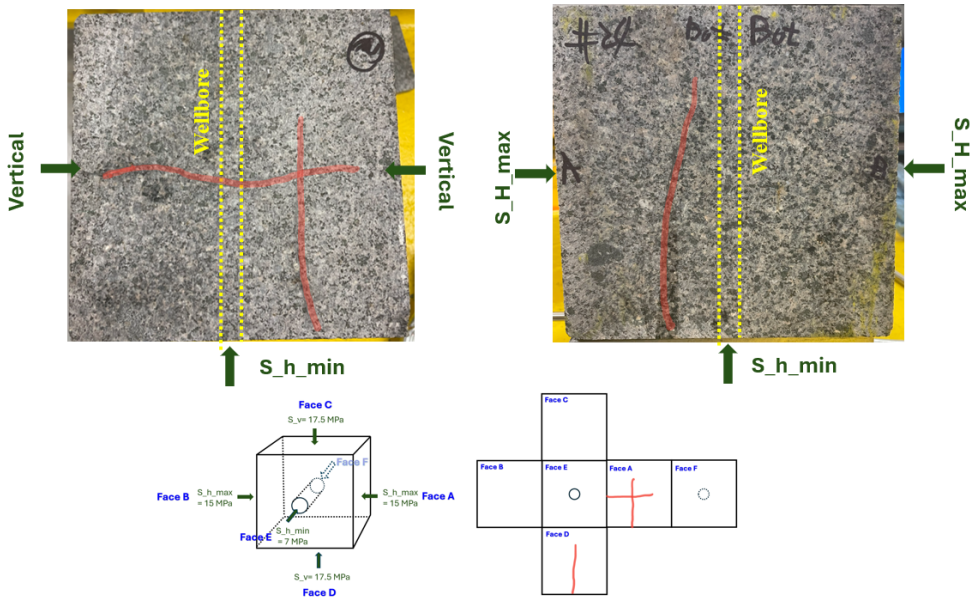

Figure 21. Observations of fracture patterns on the surface of the 6-inch cube from the HR-NTS-3 testing case.

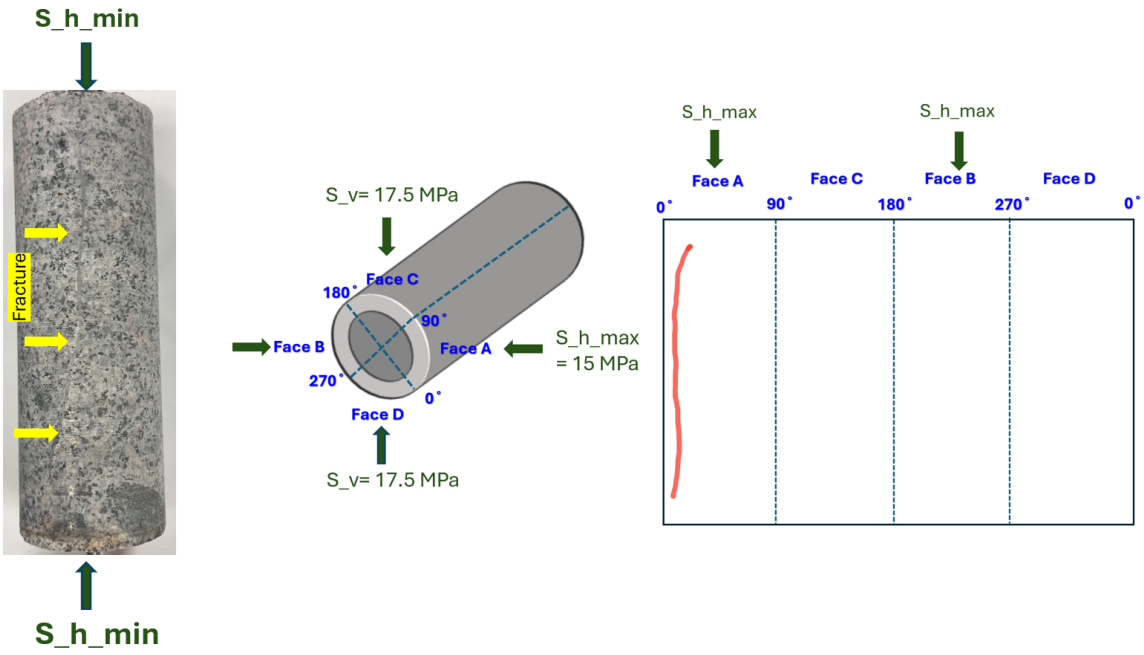

Figure 22. Observations of fracture patterns on the surface of the 2-inch core from the HR-NTS-3 testing case.

3.8 HR-NTS-4

HR-NTS-4 is a direct repeat of HR-NTS-3 with exactly the same conditions. Figure 23(a) shows the full pressure record during the four phases of stimulation: hydraulic fracturing, shut-in, reopening, and step rate. The breakdown pressure in this case is 23.2 MPa. Using the fracture compliance method, the G-function plot (Figure 23b) from the first shut-in period indicates that the closure pressure is around 12 MPa. By using the tangent method, the fracture closure pressure is picked up as 9 MPa. The reopening pressure obtained from the rapid reopening test (Figure 23c) and step rate test (Figure 23d) are approximately 12 MPa and 11 MPa, respectively. Fracture patterns observed on the surface of the 6-inch cube and on the 2-inch core are both longitudinal, as shown in Figures 24 and 25.

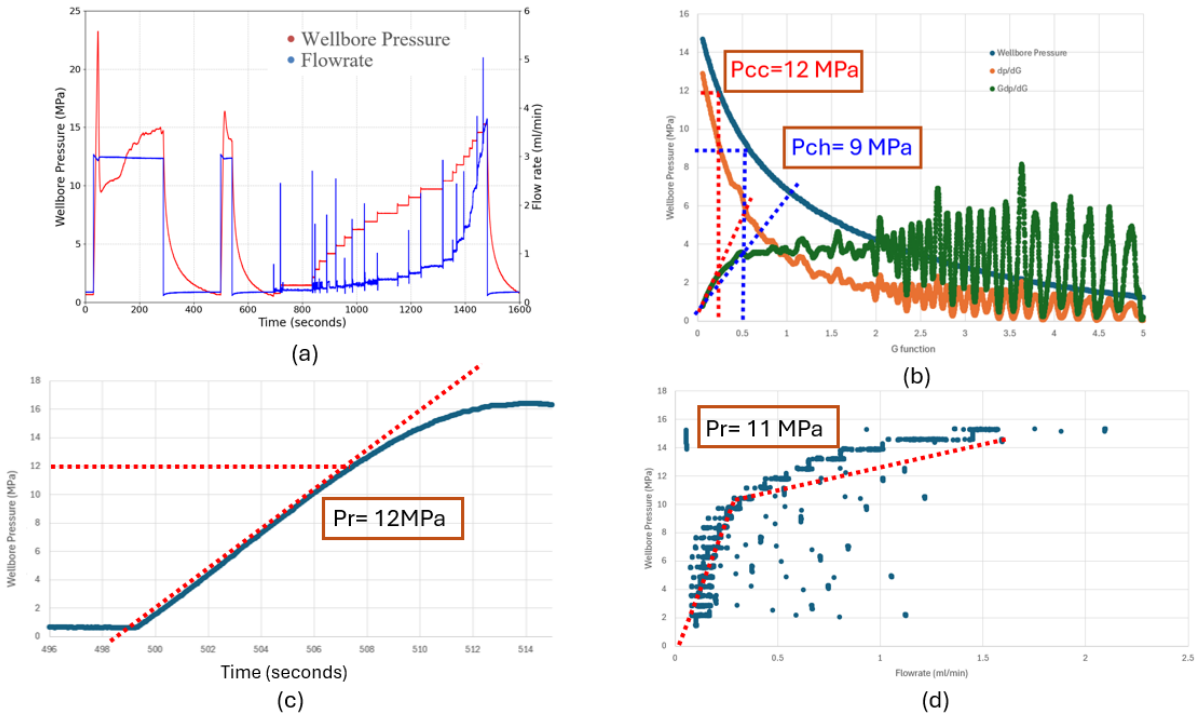

Figure 23. HR-NTS-4: (a) Full wellbore pressure record (primary y axis is the wellbore pressure and secondary y axis is flow rate); (b) G-function plot (Pcc from compliance method and Pch from tangent method); (c) Step rate plot; (d) Reopening test pressure record

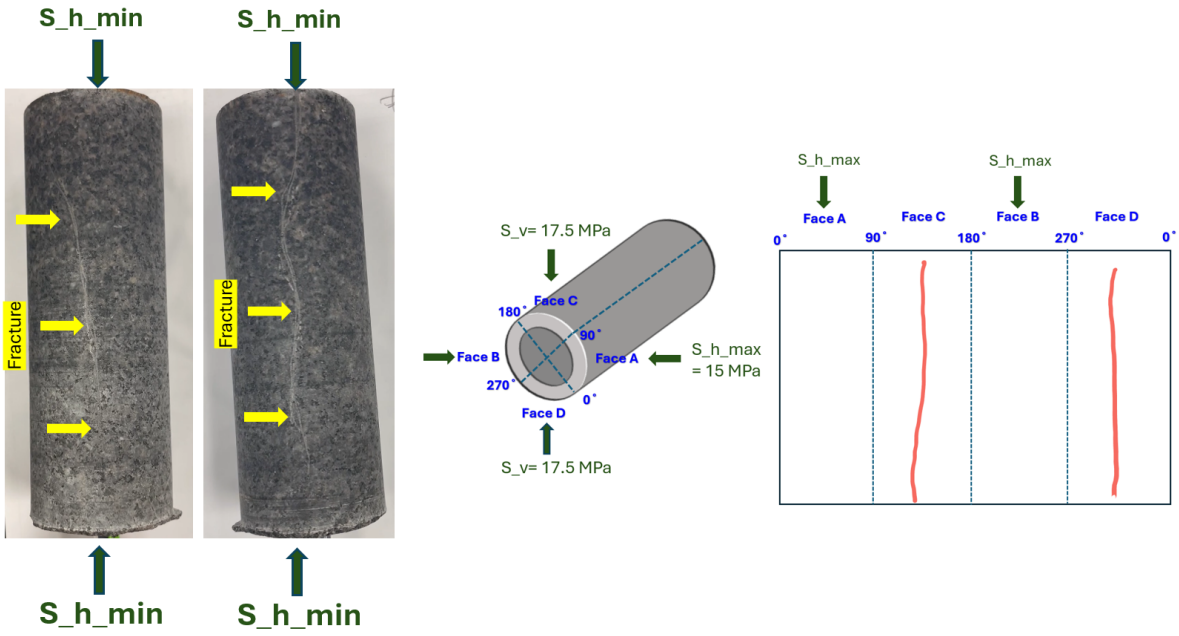

Figure 24. Observations of fracture patterns on the surface of the 6-inch cube from the HR-NTS-4 testing case.

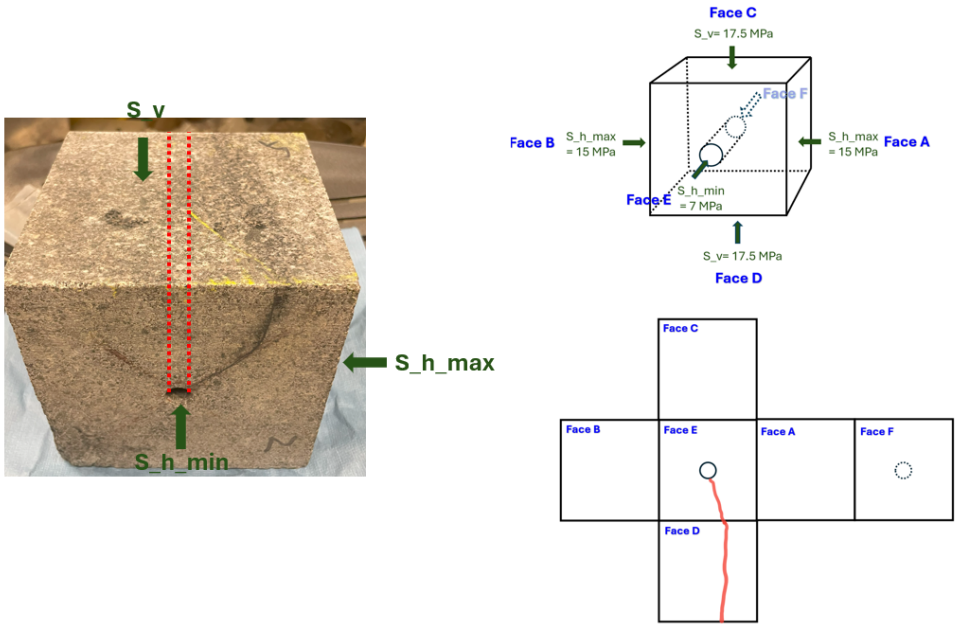

Figure 25. Observations of fracture patterns on the surface of the 2-inch core from the HR-NTS-4 testing case.

3.9 HH-ITS-5

This testing case is unique because, although all the in-situ stress values are the same as in the previous case (HH-ITS-4), the handling of thermal stress conditions is different. Unlike the HH-ITS-4 case, thermal stress is first induced by circulating room-temperature water, and the specimen is allowed to fully return to room temperature before the hydraulic fracturing phase begins. During this cooldown period, the specimen is maintained at the targeted confining stress. This design serves two purposes: first, to induce thermal stress under confining conditions, ensuring that the role of thermal stress or the thermal micro-cracks it induces is not exaggerated compared to when induced under ambient pressure conditions. Second, the extended waiting period ensures that the thermal gradient does not influence the breakdown pressure during the hydraulic fracturing phase, allowing us to isolate and assess the extent to which 'instant thermal stress' reduces tensile strength.

Figure 26(a) shows the full pressure record during the four phases of stimulation: hydraulic fracturing, shut-in, reopening, and step rate. The breakdown pressure in this case is 22.9 MPa. Using the fracture compliance method, the G-function plot (Figure 26b) from the first shut-in period indicates that the closure pressure is around 17.5 MPa. By using the tangent method, the fracture closure pressure is estimated as 16 MPa. The reopening pressure obtained from the rapid reopening test (Figure 26c) is 6 MPa. Since the flow rate data is not available for this test, thus the

step rate plotting is not showing here. Fracture patterns observed on the surface of the 6-inch cube and on the 2-inch core are both mixed, as shown in Figures 27 and 28.

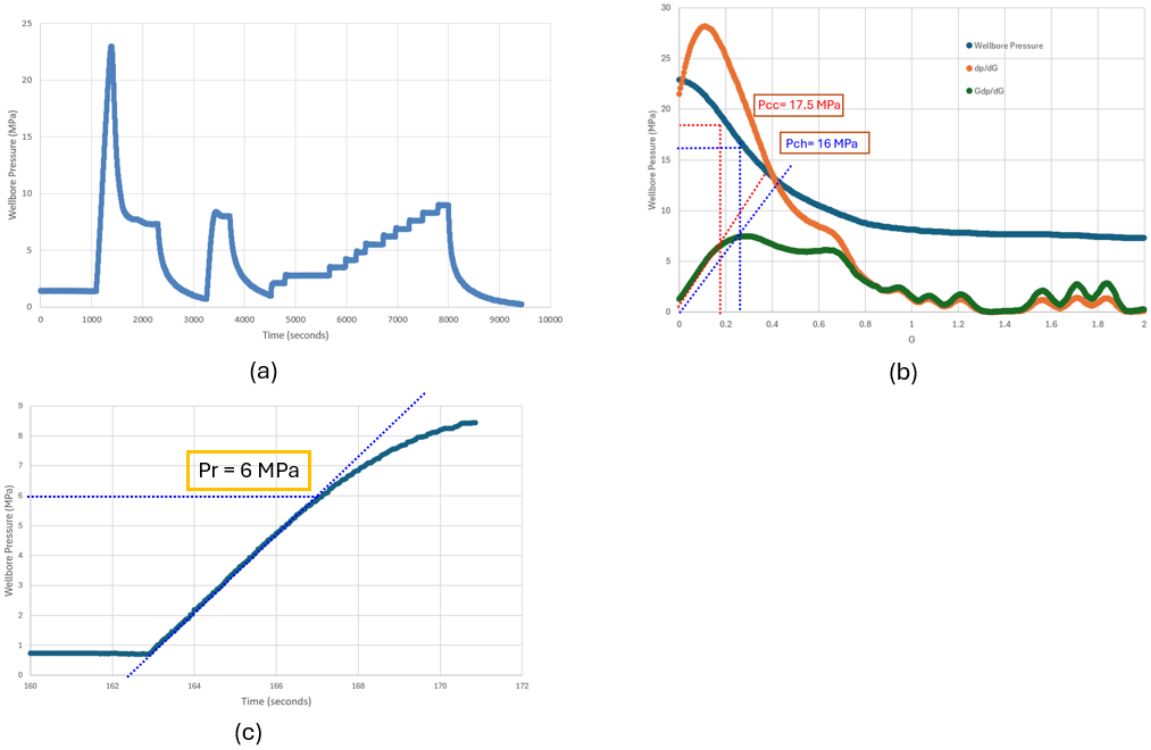

Figure 26. HH-ITS-5: (a) Full wellbore pressure record; (b) G-function plot (Pcc from compliance method and Pch from tangent method); (c) Step rate plot. Note that the flow rate data is not available for this testing case.

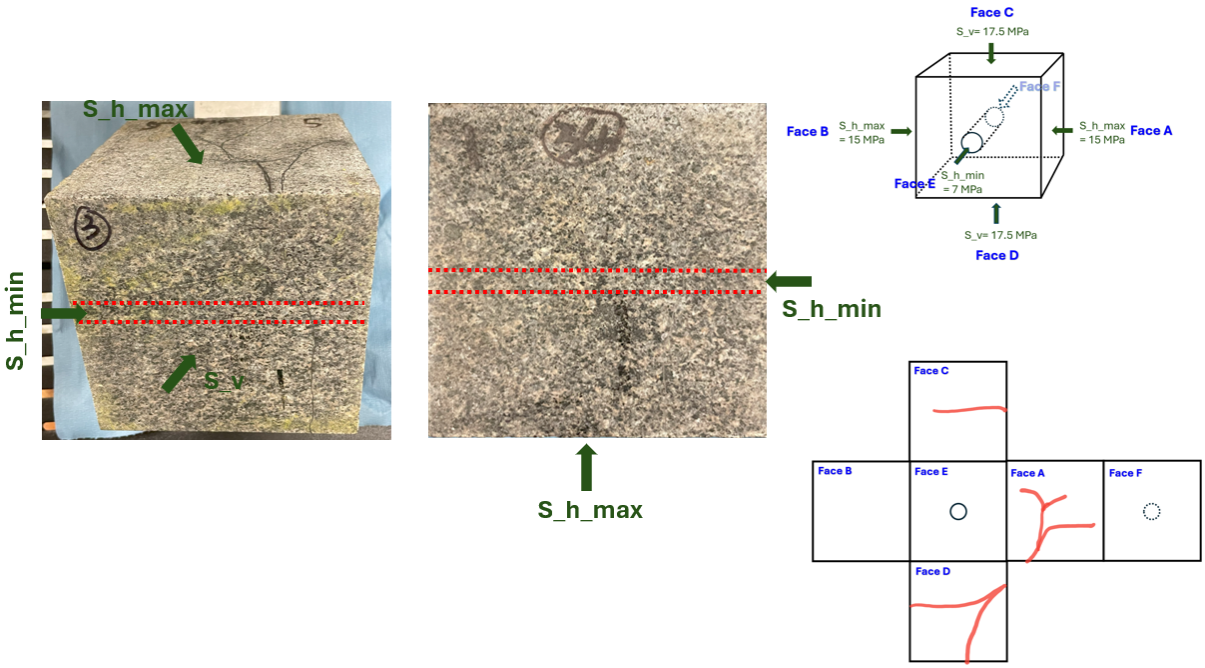

Figure 27. Observations of fracture patterns on the surface of the 6-inch cube from the HH-ITS-5 testing case.

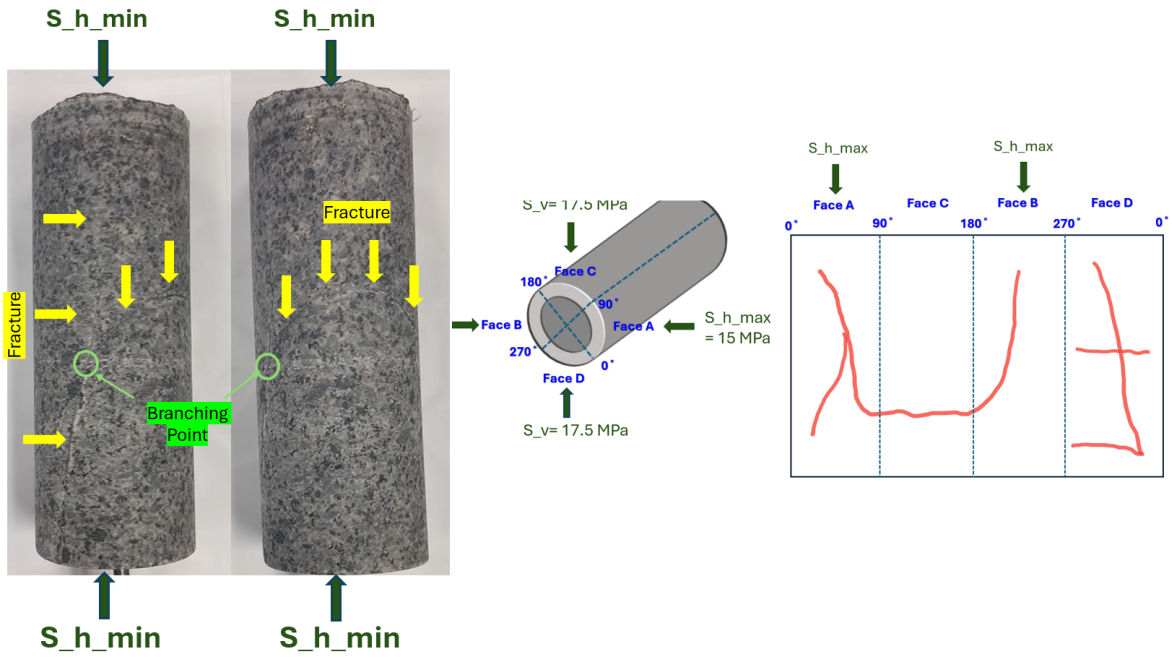

Figure 28. Observations of fracture patterns on the surface of the 2-inch core from the HH-ITS-5 testing case.

4. Discussions

All the details of the experimental data presented individually in the last session are summarized in Table 1. By comparing the different breakdown pressures from the contrasting cases of HH-ITS-2, HH-ITS-3, and HR-NTS-1 and HR-NTS-2, as shown in Figure 29, where all experimental conditions remained the same except for the thermal stress stimulation in the first two cases and the lack of thermal stress stimulation in the latter two cases, we first found that the breakdown pressure was significantly reduced from an average of 40 MPa to 16.4 MPa by the thermal stimulations. A similar trend can also be observed when comparing the breakdown pressures obtained from HH-ITS-4 and HR-NTS-4, as shown in Figure 30, where the only difference is the thermal stress conditions. The breakdown pressure in the no-thermal stimulation case is 23.3 MPa, whereas the breakdown pressure in the thermal stimulation case is 15 MPa.

Table 1. Overall Summary of Experimental Data for Both Vertical and Horizontal Testing Cases in the Current Milestone Report

Testing Case	Breakdown Pressure (Mpa)	Closure Pressure (MPa) -G function- Compliance Method	Closure Pressure (MPa) -G function- Holistic	Reopening Pressure (MPa)- Reopen	Reopening Pressure (MPa) - Step Rate	Applied Vertical Stress	Applied Horizontal Maxumum Stress	Applied Horizontal Minimum Stress	Thermal Sterss Effect
VR-NTS-1	18	--		--	--	17.5	15	10	N
VH-NTS-1	23.2	14	7	14.2	7.8	17.5	15	10	N
VH-NTS-2	21.8	11	8	13.8	11.5	17.5	15	10	N
VH-NTS-3	22.4	13.5	11	22.5	15.8	17.5	15	10	N
VH-ITS-1	20.6	12	8	13.5	10	17.5	15	10	Y
VH-ITS-2	17.7	13	8	10	10.5	17.5	15	10	Y
IH-ITS-1	15.7	11.5	6.2	11	11	17.5	15	11.8	Y
IH-ITS-2	8.7	7	4	8.5	8.5	17.5	15	11.8	Y
HH-ITS-1	23.1	15	14	18	15.5	17.5	15	10	Y
HH-ITS-2	21.4	7.5	5.5	10	10	17.5	15	3	Y
HH-ITS-3	11	6	4	5	5	17.5	15	3	Y
HH-ITS-4	15	10	7	9	9	17.5	15	7	Y
HH-ITS-5	22.9	17.5	16	6	--	17.5	15	7	Y
HR-NTS-1	37.5	11	6.5	12	11	17.5	15	3	N
HR-NTS-2	42.5	11	7.8	14	13	17.5	15	3	N
HR-NTS-3	20.4	7.5	4.8	7	7	17.5	15	7	N
HR-NTS-4	23.2	12	9	12	11	17.5	15	7	N

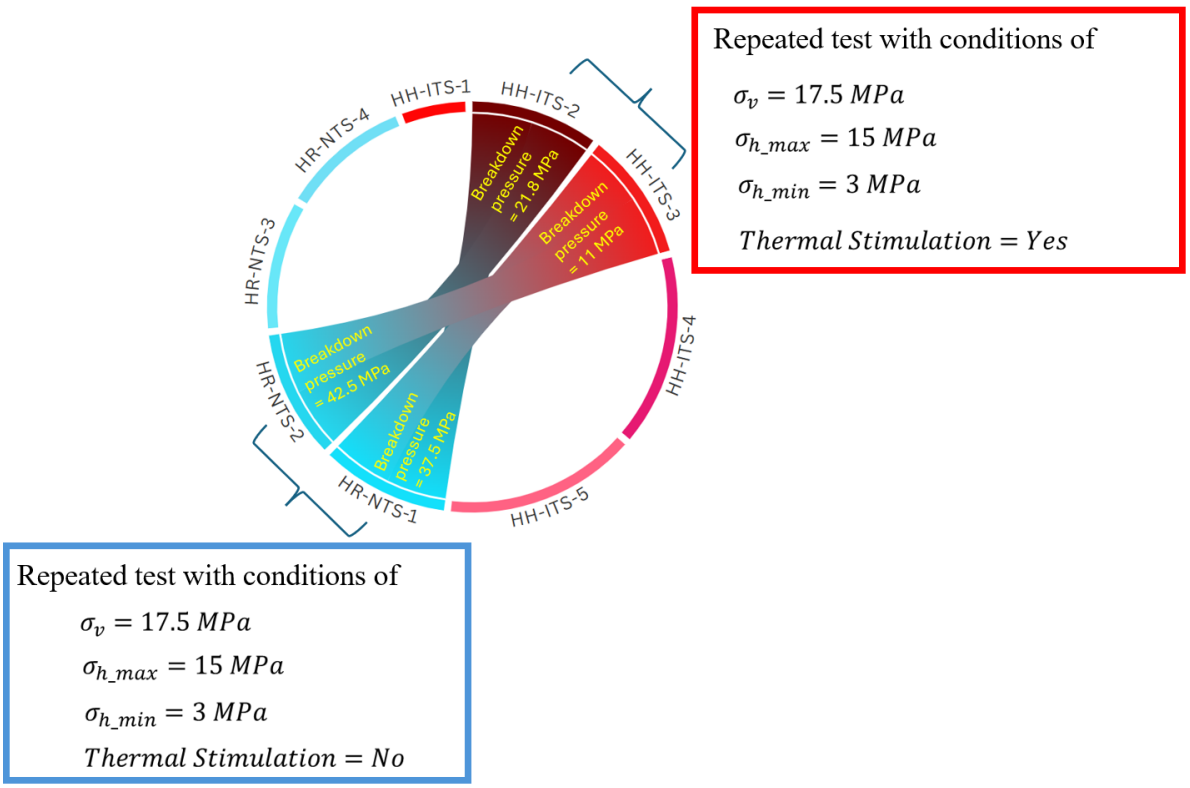

Figure 29. Comparison testing case of HH-ITS-2 and 3 with HR-NTS-1 and 2.

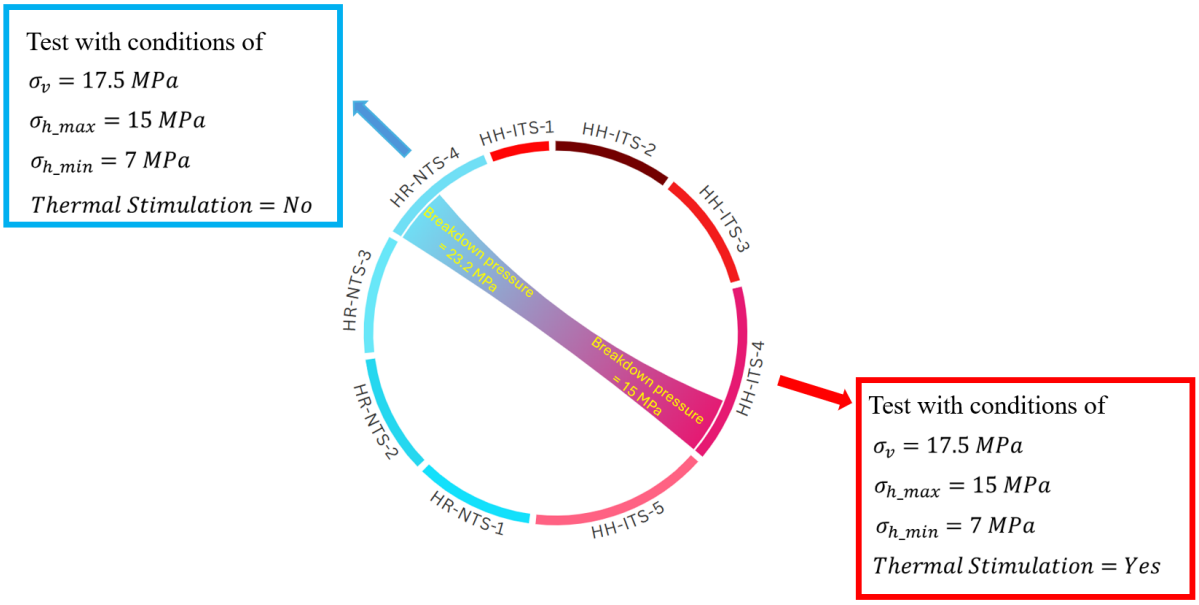

Figure 30. Comparison testing case of HH-ITS-4 with HR-NTS-4.

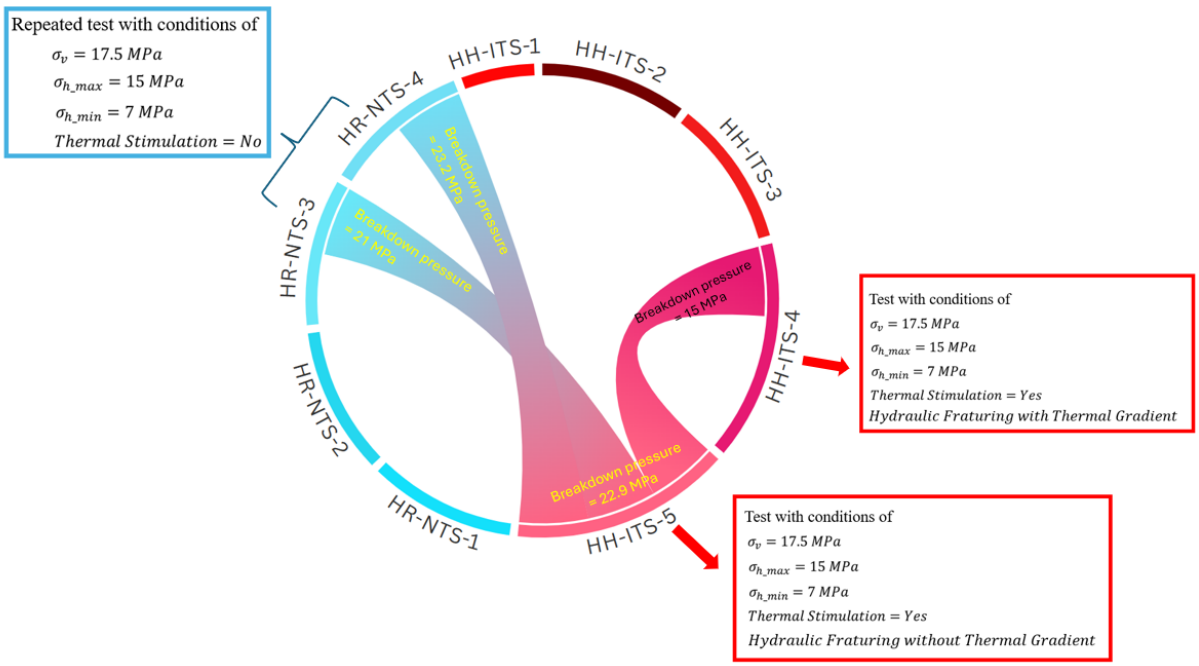

Figure 31. Comparison testing case of HH-ITS-4 with HH-NTS-5 and HH-ITS-5 with HR-NTS-3 and 4.

Even though the mechanisms leading to the reduction in breakdown pressure remain unclear, the experimental data obtained so far provides some thoughts. By comparing the testing cases of HH-ITS-4 and HH-ITS-5, as shown in Figure 31, the only difference lies in the timing and thermal conditions when hydraulic fracturing is initiated. In the HH-ITS-4 case, hydraulic fracturing is started immediately after circulation is stopped (approximately 20 minutes), during which a strong thermal gradient, induced by the circulation, still exists within the testing samples. In contrast, for the HH-ITS-5 case, the hydraulic fracturing phase does not begin until the testing sample has completely returned to room temperature (after 48 hours of stopping the injection), at which point the thermal gradient within the sample has entirely disappeared. By comparing the breakdown pressures from these cases, as shown in Figure 31, we observe that the breakdown pressure for the HH-ITS-5 case (22.9 MPa) falls within a similar range as the breakdown pressures for the HR-NTS cases (#3 and #4, which are 21 MPa and 23.2 MPa, respectively). However, the breakdown pressure for HH-ITS-4 is 15 MPa, which is significantly lower than that of the no-thermal-stimulated cases. This leads to the assumption that the breakdown pressure is reduced by a thermal-gradient-related THM coupling process during the hydraulic fracturing process. However, further repeated tests are needed to confirm this assumption.

Interestingly, if we further compare the fracture patterns from the same group mentioned above from Figure 29 (HH-ITS-2, HH-ITS-3, HR-NTS-1, and HR-NTS-2), based on observations of the 2-inch cores, the no-thermal stimulation testing cases tend to favor longitudinal fracture patterns. In contrast, under the same in-situ stress conditions but with thermal stimulations,

transverse fracture patterns are more favorable, sometimes co-existing with longitudinal fractures. This is also evident from the SEM observations of the inner surface of the wellbore for the thermally stimulated sample, as shown in Figure 32 where a branching point is captured. The same observations are evident when comparing HH-ITS-4 and HR-NTS-4 as mentioned in Figure 30, where the only difference is the thermal stimulation. For the no-stimulation testing scenario, horizontal fractures are generated in the 2-inch core, whereas longitudinal fractures are more favorable when thermal stimulation is applied. Furthermore, this phenomenon persists even after the thermal gradient has completely dissipated. In such cases, the fractures exhibit a mixed type, with longitudinal fractures co-existing with transverse fractures on the 2-inch core, as observed in the HH-ITS-5 test.

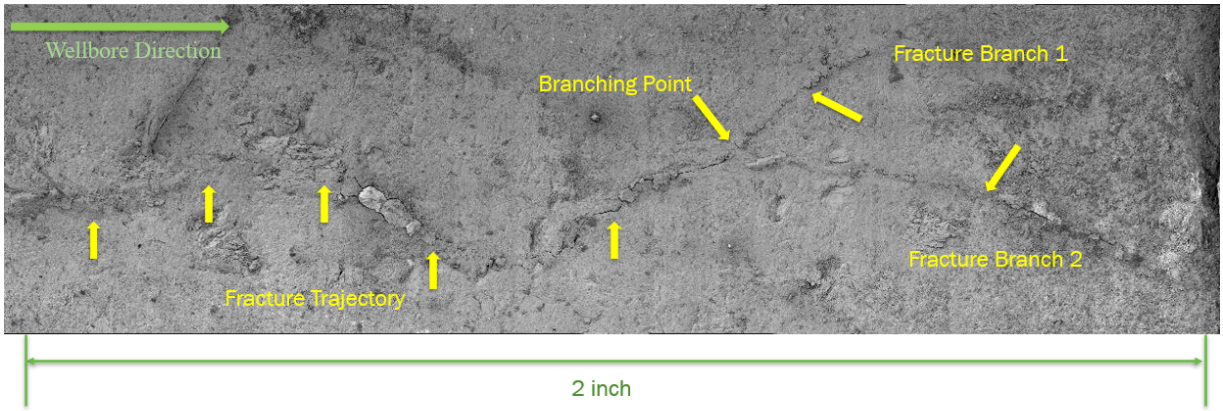

Figure 32. SEM fracture observations on the wellbore surface from vertical well-high temperature sample-induced thermal stress

If we summarize the classification of fracture categories from all the vertical and horizontal wells in Figure 33, it becomes evident how thermal stimulation can potentially alter fracture patterns. Originally longitudinal fractures in both vertical and horizontal wells can transform into either pure transverse fractures or a mixed type, where transverse and longitudinal fractures co-exist.

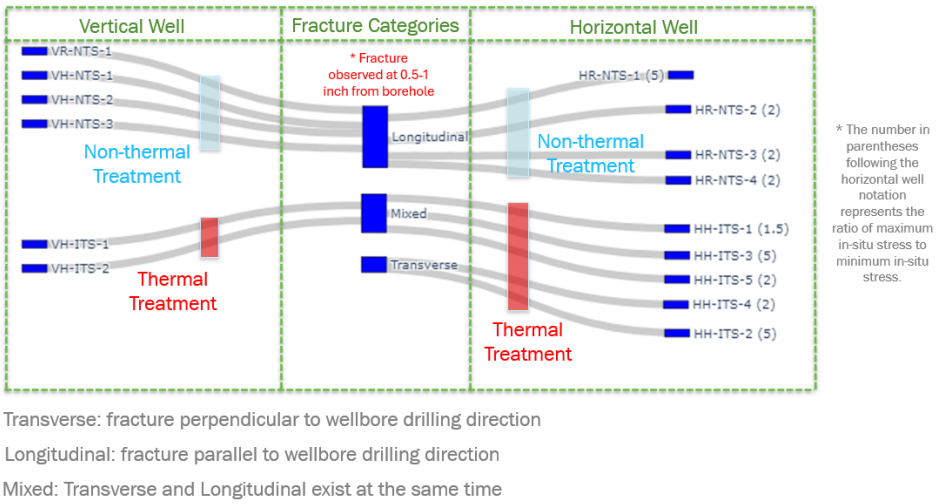

Figure 33. Classification of fracture categories in vertical and horizontal wells under thermal and no-thermal treatments.

Based on the literatures, one of the difficulties for the in-situ stress estimation originates from overly simplistic models and assumptions used for in-situ data interpretation, such as basic fracture geometry and the presumption that the entire fracture face closes simultaneously (Cornet, 1981; BC Haimson et al., 2003; Bezalel Haimson et al., 1967; Ito et al., 1999). Classic interpretation of σ_H and σ_h from hydraulic fracturing stress tests typically hinges on three components (Hubbert and Willis, 1957): 1. the breakdown stress (p_b), that is, the peak value observed in wellbore pressure evolution; 2. the shut-in pressure, equivalent to the fracture closure pressure (p_c), indicating the fluid pressure at which the crack uniformly closes onto itself; 3. the reopening pressure (p_r), where the initiation pressure corresponds to zero tensile strength. The complexities mentioned above profoundly influence the borehole pressure history recorded during fracturing tests, resulting in less clear interpretations and open debates and questions about determining these three pressure components. However, generally, it is considered that a reliable estimate of the minimum horizontal principal stress (σ_h) equals the closure pressure (p_c) when the hydraulic fractures initiate and propagate in a plane normal to σ_h. The determination of the larger horizontal stress (σ_H), however, is a more complex process and involves greater uncertainties (Ito et al. 1999). It is typically inferred from p_b, p_r, and σ_h, using a wide array of proposed theories, experimental data, and field experiences. For example, an expression presented by Hubbert and Willis (1957),

$$p_b = 3\,\sigma_h - \sigma_H + \sigma_t, \quad (1)$$

where σ_t is tensile strength of the material, was further refined by Haimson and Fairhurst (1967) into

$$p_b = (3\,\sigma_h - \sigma_H + \sigma_t)/2, \quad (2)$$

which integrates the poroelastic effects. Later, Ito et al. (1999) put forth the equation of reopening pressure as

$$p_r = 3\,\sigma_h - \sigma_H. \quad (3)$$

They also pointed out the value of reopening pressure is more or less equivalent in value of ISIPs, which further provided the field tests and laboratory experiments as the evidences (Cheung et al., 1989; Evans et al., 1989; Lee et al., 1989). Further building on the elastic theory and Kirsch's solution, the maximum horizontal stress can be related to reopening pressure via (BC Haimson et al. (2003)

$$\sigma_H - p_0 = 3(\sigma_h - p_0) - (p_r - p_0), \quad (4)$$

where p_0 is pore pressure. While the aforementioned approaches are widely used in field measurement campaigns, their validity and reliability can sometimes be open to discussion, particularly under certain conditions. These scenarios may involve, for example, when the fracture show more complexities rather than the sample geometry and when the fractures are not complete close after the each pressure cycle (Bredehoeft et al., 1976; Cornet, 1981; Gronseth et al., 1981).

If we apply Eq.3 to obtain the predicted reopening pressure based on the horizontal minimum stress and horizontal maximum stress that were actually applied in the experiment and plot them along with the reopening pressure obtained from the extended post-peak in Figure 34, we can easily find that for all the horizontal well cases, the reopening pressure from Eq.3 underestimates the reopening pressure by up to 50%. Note that for the small horizontal minimum stress case, equal to 3 MPa, Eq.3 predicts a negative reopening pressure, as shown in Table 2. For most of the vertical well cases, the theoretical prediction overestimates the reopening pressure by up to 30%.

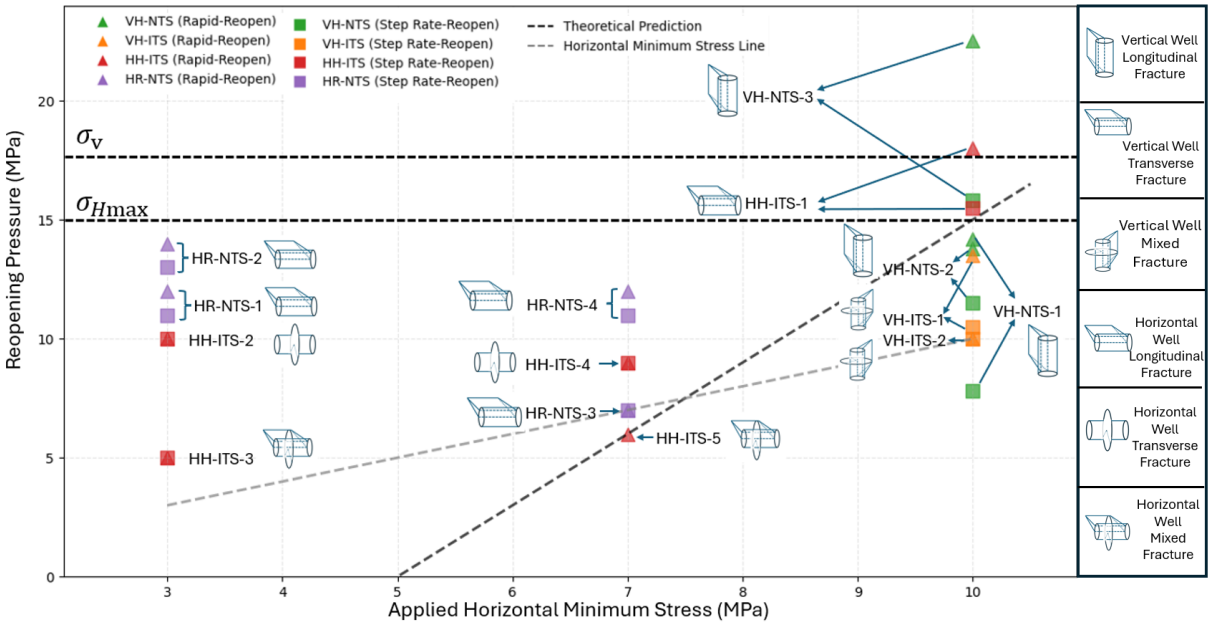

Figure 34. Comparison of closure pressures obtained from the experiment versus the predicted values from the theoretical from equation 3.

Table 2. Percentage Deviation between Experimental and Theoretical Reopening Pressures

Testing Case	Average Closure Pressure (MPa)	Theoretical Value (MPa)	Deviation Percentage (%)
VH-NTS-1	11.0	15	-26.7
VH-NTS-2	12.9	15	-14.0
VH-NTS-3	19.2	15	27.7
VH-ITS-1	10.5	15	-30.0
VH-ITS-2	10.8	15	-28.3
HH-ITS-1	16.8	15	11.7
HH-ITS-2	10.0	-6	-266.7
HH-ITS-3	5.0	-6	-183.3
HH-ITS-4	9.0	6	50.0
HH-ITS-5	9.0	6	50.0
HR-NTS-1	11.5	-6	-291.7
HR-NTS-2	13.5	-6	-325.0
HR-NTS-3	7.0	6	16.7

From our experiment, the post-peak pressure extended protocol procedures have enabled us to simulate the DFIT test from the field, which uses the shut-in period of pressure records and the G-function plot to estimate the fracture closure pressure. Regarding the fracture closure pressure estimations using the G-function, there are two prevalent methods: the fracture compliance method and the holistic method, also known as the tangent method (McClure et al., 2019, Guglielmi et al., 2023, Barree et al. 2009). The difference lies in the fact that the fracture

compliance method identifies the closure pressure from the early deviation of the GdP/dG vs. G-time plot, based on the belief that fracture walls first begin to come into contact, causing increased fracture stiffness (McClure et al., 2016, Ye and Ghassemi et al., 2023). As soon as the fracture faces start touching, the mechanical properties (compliance) of the system begin to change. In contrast, the tangent method waits until the complete closure process is finished, with the closure points typically being picked at a later stage or at a large G value (McClure et al., 2019). As shown in Figure 35, our experimental data demonstrate that using the fracture compliance method consistently provides a higher fracture closure estimation than the tangent method.

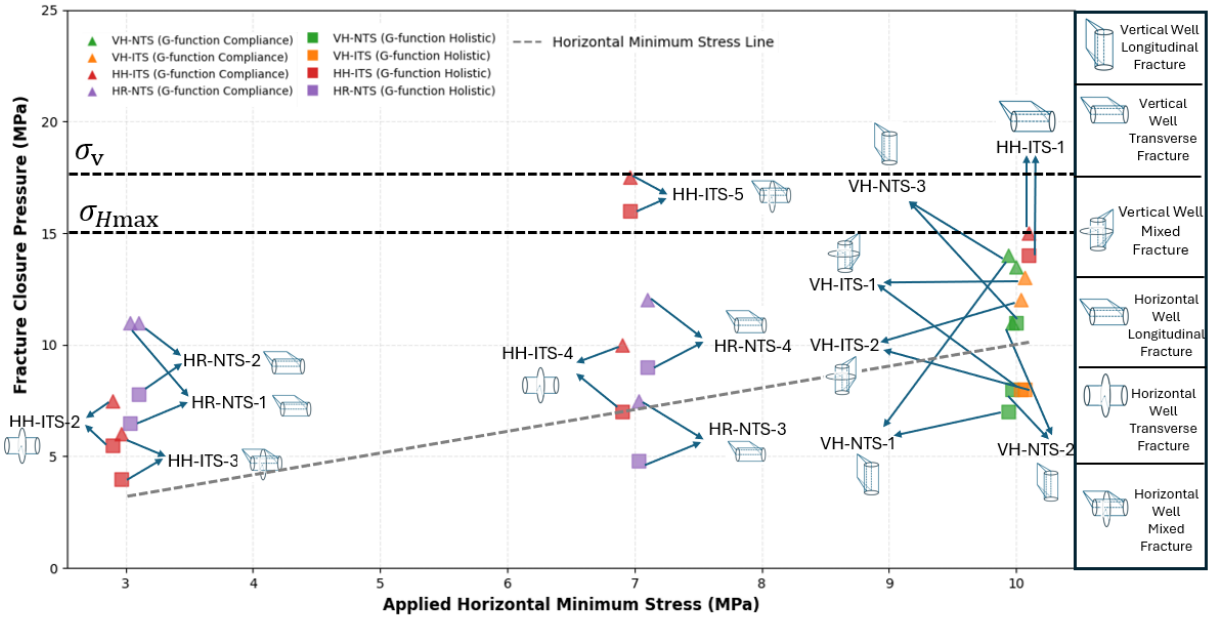

Figure 35. Comparison of closure pressures obtained using the fracture compliance method and the tangent method (holistic method) from the shut-in pressure data. Note that some data points have been slightly shifted horizontally to avoid overlapping and improve visibility. Exact values can be referenced in Table 1.

5. Conclusions & future work

To date, we have successfully completed 17 hydraulic fracturing tests, which addressed six combined scenarios relevant to Utah FORGE conditions. These tests have investigated the effects of various well directions, in-situ stress regimes, and thermal stress conditions on fracture patterns and trajectories. The data obtained from these experiments have provided valuable insights into three main preliminary research findings: firstly, how cooling circulation affects breakdown pressure; secondly, the potential roles of thermo-elastic stress and thermally induced micro-fractures in influencing favorable fracture patterns; and thirdly, the accuracy of the current prevalence of in-situ stress and reopening pressure estimation theory.

Based on the evidence obtained so far, we have found that thermal stimulation not only induces a strong thermal gradient, leading to thermal stress and a THM-coupled process, but can also potentially create thermally induced micro-fractures. So far, the experimental data have shown that the thermal gradient and thermal fractures may play different roles during the hydraulic fracturing phase. The thermal gradient and its associated THM coupling process appear to play an important role in reducing breakdown pressures, while the thermal stress-induced micro-fractures may significantly influence favorable fracture patterns. Furthermore, the complexity of the EGS reservoir stimulation process and its high-temperature characteristics pose remarkable challenges to the current prevalence of reopening pressure estimation theory, causing deviations of up to 50% of the reopening pressure estimation.

Building on this groundwork, we will continue conducting an extensive series of experiments to obtain repeated experimental evidence to confirm the current findings and conduct deeper investigations to explore the unsolved questions discovered and proposed within this report. At the same time, we will collaborate with the modeling team to provide the mechanical properties needed for numerical simulations. The primary goal of all the endeavor is to expand the experimental database, systematically uncovering and addressing the complexities inherent in inferring in-situ stresses within Enhanced Geothermal Systems (EGS) reservoirs. Ultimately, as proposed in the SOPO, this experimental database will facilitate experimental throughput to provide stochastic data on fracture branch frequencies and orientations. These data will enable the generation of probabilistic mappings between fracture geometry and in-situ stresses. Such probabilistic fracture maps can be used both for model validation and for direct comparison with Utah FORGE post-fracturing image logs.

Acknowledgement

This work was performed at the University of Pittsburgh with funding provided by the DOE EERE Geothermal Technologies Office to Utah FORGE and the University of Utah under the project 'Enhanced Geothermal System Concept Testing and Development' at the Milford City, Utah Frontier Observatory for Research in Geothermal Energy (Utah FORGE) site. Support was received via Subcontract No. B651948.

Parts of this work were performed under the auspices of the U.S. Department of Energy by Lawrence Livermore National Laboratory under Contract DEAC52-07NA27344.

Additional support for APB is provided by the RK Mellon Faculty Fellowship in Energy. We would like to express our gratitude to Charles Hager (PITT) for his outstanding technical contributions. We are also thankful for the support of our entire research group at the Hydraulic Fracturing Lab here at the University of Pittsburgh, particularly Olivia Hartz, Tess Harper, and Jared Broscious.

References

Hubbert, M. K., & Willis, D. G. (1957). Mechanics of hydraulic fracturing. Transactions of the AIME, 210(01), 153-168.

Cornet, F. (1981). Analysis of injection tests for in-situ stress determination. Paper presented at the Workshop on Hydraulic Fracturing Stress Measurements, California, US.

Haimson, B., & Cornet, F. (2003). ISRM suggested methods for rock stress estimation—part 3: hydraulic fracturing (HF) and/or hydraulic testing of pre-existing fractures (HTPF). International journal of rock mechanics and mining sciences, 40(7-8), 1011-1020.

Haimson, B., & Fairhurst, C. (1967). Initiation and extension of hydraulic fractures in rocks. Society of Petroleum Engineers Journal, 7(03), 310-318.

Ito, T., Evans, K., Kawai, K., & Hayashi, K. (1999). Hydraulic fracture reopening pressure and the estimation of maximum horizontal stress. International journal of rock mechanics and mining sciences, 36(6), 811-826.

Barree, R. D., Barree, V. L., & Craig, D. P. (2009). Holistic fracture diagnostics: consistent interpretation of prefrac injection tests using multiple analysis methods. SPE Production & Operations, 24(03), 396-406.

McClure, M. W., Jung, H., Cramer, D. D., & Sharma, M. M. (2016). The fracture-compliance method for picking closure pressure from diagnostic fracture-injection tests. *Spe Journal*, *21*(04), 1321-1339.

Guglielmi, Y., McClure, M., Burghardt, J., Morris, J. P., Doe, T., Fu, P., ... & Zoback, M. D. (2023). Using in-situ strain measurements to evaluate the accuracy of stress estimation procedures from fracture injection/shut-in tests. *International Journal of Rock Mechanics and Mining Sciences*, *170*, 105521.

Ye, Z., & Ghassemi, A. (2023, August). Reexamining in-situ stress interpretation using laboratory hydraulic fracturing experiments. In *Unconventional Resources Technology Conference, 13–15 June 2023* (pp. 305-315). Unconventional Resources Technology Conference (URTeC).

Mcclure, M., Fowler, G., & Picone, M. (2022, January). Best practices in DFIT interpretation: Comparative analysis of 62 DFITs from nine different shale plays. In *SPE International Hydraulic Fracturing Technology Conference and Exhibition* (p. D031S011R001). SPE.

McClure*, M., Bammidi, V., Cipolla, C., Cramer, D., Martin, L., Savitski, A. A., ... & Voller, K. (2019, October). A collaborative study on DFIT interpretation: Integrating modeling, field data, and analytical techniques. In *Unconventional Resources Technology Conference, Denver, Colorado, 22-24 July 2019* (pp. 2020-2058). Unconventional Resources Technology Conference (URTeC); Society of Exploration Geophysicists.